



A critical review on the fused deposition modeling of thermoplastic polymer composites

Pavan Kumar Penumakala^{*}, Jose Santo, Alen Thomas

Department of Mechanical Engineering, Birla Institute of Technology and Science-Pilani, Hyderabad Campus, 500078, India

ARTICLE INFO

Keywords:

Fused deposition modeling
Fused filament fabrication
Thermoplastics
Polymer composites
3D printing

ABSTRACT

Fused Deposition Modeling (FDM) is a widely used additive manufacturing technology for fabrication of complex geometric parts using thermoplastic polymers. The quality issues and inferior properties of fabricated parts limited this process to manufacture parts for industrial level applications. Reinforcing the polymer with nanoparticles, short fibers or continuous fibers improve mechanical, thermal and electrical properties compared to the neat polymer. Several works have been carried out since last two decades to print quality products through FDM by using composite materials. The success of expanding this technique to industrial applications depends on the preparation of printable composite feedstock filament and printing without defects. This article reviews the challenges involved in the preparation of composite feedstock filaments and printing issues during the printing of nano composites, short and continuous fiber composites. The printing process of various thermoplastic composites ranging from amorphous to crystalline polymers is discussed. Also, detailed explanation is given about the analytical and numerical models used for simulating the FDM printing process and for estimating the mechanical properties of the printed parts. This critical review mainly helps the young researchers working in the area of processing of composite materials via 3D printing.

1. Introduction

Fused Deposition Modeling (FDM), a layer-wise 3D printing technology, has been developed by Stratasys © for fabricating complex geometrical parts [1]. Among different additive manufacturing processes, FDM became more popular due to low cost and flexibility to use different materials. Over the years, this process has been used for making products from a wide range of materials such as plastics, metal powder, ceramics and composites [2,3] for aerospace [4], medical [5], mold design [6] and automobile applications [7]. In this process, filament material is extruded through a heated nozzle and deposited layer-by-layer in the semi-solid state on a partially constructed part. As shown in Fig. 1, the process consists of a build platform, print bed, liquefier head and build material spool. First, part model's STL file format that has to be fabricated is created in the geometry creation software. Then, it is imported to the software in which it is sliced into thin two-dimensional layers. The tool path motion is generated using this two-dimensional contour information. A 3-axis system controls the movement of the liquefier head. It moves in the X-Y plane as per the tool path made by the software and deposits the first layer. After completing

one layer, the head moves downward in the z-direction by an amount of set layer thickness. The newly added layer fuses with the already deposited layer and forms a bond. Successive layers of the material deposition will occur until the entire part finishes. After the completion, the structure can be taken out from the print bed manually or chemically removing the support structure [8]. According to the ASTM F42 (Additive Manufacturing Technologies) terminology, this process could also be termed as Fused Filament Fabrication (FFF) or material extrusion additive manufacturing (AM).

Initially, FDM printed parts have been used for low load prototypes such as domestic toy applications. With technological advancements, the process is extended nowadays to print parts for real time industrial applications. Large scale geometries of several meters of length and width are recently printed at very high material output rates of more than 200 kg/h [9]. The Big Area Additive Manufacturing (BAAM) system developed at Oak Ridge National Laboratory (ORNL) in collaboration with Cincinnati Incorporated© can print large scale geometries with dimensions of several meters. The design principle of BAAM is similar to FFF. The nozzle size and diameter are much bigger than lab scale printers. Also, polymer pellets are fed to the extruder feeding system,

* Corresponding author.

E-mail address: pavankp@hyderabad.bits-pilani.ac.in (P.K. Penumakala).

instead of filaments. The extruder is controlled by gantry to print different sizes. Similarly, Thermwood® developed Large Scale Additive Manufacturing System (LSAM). This system contains CNC machine in addition to FFF printer, to machine the printed parts. Readers are suggested to refer company websites to see illustrations of these big scale machines and printed parts [10,11]. The research group in Spain also developed large format Polymeric Pellet-Based Additive Manufacturing (PPBAM) system for printing different polymeric parts for Naval applications [13]. Continuous research is going on to print parts by FFF for more industrial applications. Composite Additive Manufacturing Research Institute (CAMRI) was developed at Purdue university to print different high performance polymer composites for tooling applications [12].

The quality of the printed parts depends on various underlying physical phenomena during printing, which are highlighted in Fig. 1. The part integrity and properties depend highly on bonding phenomena and bond quality. The bond formation between two layers includes surface contacting, neck growth and molecular diffusion [14–16]. This bonding phenomena occur between the adjacent filaments in a layer (intra-layer) and among the successive layers (inter-layer). Gurrala et al. demonstrated that during the bonding process, the total time available for solidification is less and partial neck growth and coalescence occurs resulting in the void formation between layers [17]. Due to the formation of voids, the strength of the FDM parts is quite low when compared to the parts made by other processes such as injection molding. Also, the difference in temperature profiles between adjacent layers during the solidification cause shrinkage, residual stress and distortion of the printed part. The built chamber temperature is a critical factor in FDM process. The difference between the filament temperature and the built chamber temperature causes additional thermal stresses and warpage. Often, the built chamber is also heated to a high temperature to minimize thermal stress.

To improve the properties of the FDM printed parts, literature works focused on developing composite material systems by reinforcing different fillers to the base polymer and printing of these composites [18, 19]. Parts made using these composites found to exhibit higher mechanical, thermal and electrical properties compared to the

unreinforced polymer printed parts. Driven by new applications and challenges, the FDM technology keeps growing in producing components made of new composite material systems [20]. The properties of composite materials are highly sensitive to the reinforcement type, i.e., particle, short fiber or continuous fiber. Also, the reinforcement size, shape and distribution affect the properties. Generally, in the case of nano particles, more than 8–10 wt% may decrease the properties due to agglomerates formation. Short fiber composites show a decrement in properties at loadings higher than 30 wt%. During the FDM printing of short fiber or particle reinforced composites, the orientation of fibers in the extruding nozzle and in the print layer depends on the flow field in the liquefier and in the nozzle [21]. The reinforcement size alters the melt viscosity, which effects the flow field. The nozzle may act as a filter for higher particle sizes, which causes the nozzle blockage after few prints. Few thermal and electrical properties of 3D printed parts using short-fiber composites have been improved [22]. However, the mechanical performance of printed parts with particle or short fiber composites are still inferior to the parts made using other short fiber composite processing techniques such as compression molding [23].

The mechanical performance of continuous fiber reinforced composites is higher compared to short fiber composites. Few works focused on the 3D printing of continuous fiber reinforced composites. Matsuzaki et al. proposed a new method for the first time for printing continuous fiber composites using an in-nozzle impregnation technique. In this, the thermoplastic resin and preheated reinforcing fibers are supplied from two separate rollers and are impregnated in the heated nozzle [24]. The heated resin inside the nozzle consolidates the fibers. These impregnated fibers are extruded from the nozzle, as shown in Fig. 2a. These modifications to the nozzle system offers the advantage of printing different fiber and resin combinations. In this work, continuous fiber reinforced composites have been printed by reinforcing carbon fibers in polylactic acid (PLA). The modulus and strength of the 3D printed continuous carbon fiber reinforced composites is higher compared to the conventional 3D printed composites. Few other works have been presented to print continuous fiber reinforced composites by modifying traditional FDM printers [25,26]. Printing through this in-nozzle impregnation technique has less control over the fiber volume fraction in the printed

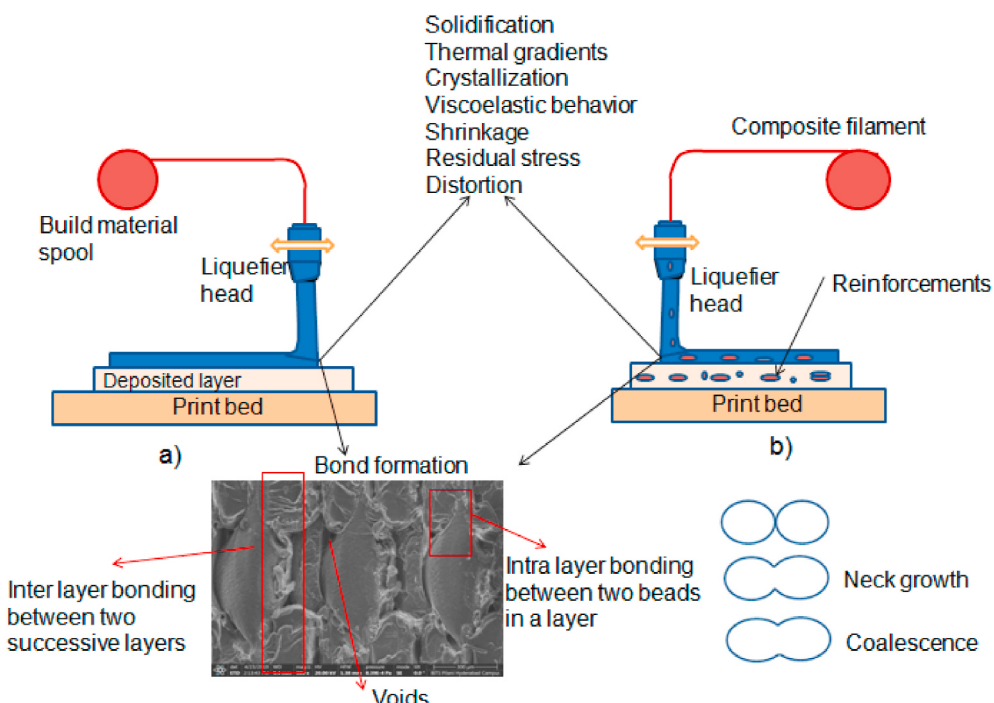


Fig. 1. Schematic and illustration of different physical phenomena during FDM process: a) printing of neat polymer b) printing of polymer reinforced with particle fillers or short fibers.

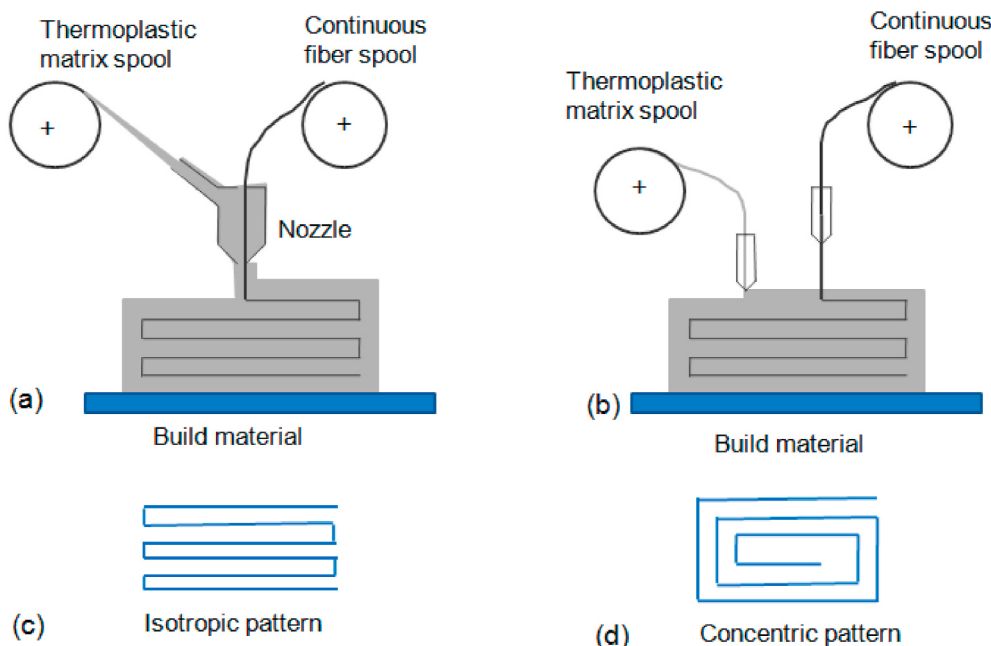


Fig. 2. Schematic of FDM process using continuous fiber reinforcement a) in-nozzle impregnation b) printing with two separate nozzles c) isotropic and d) concentric pattern of fibers during printing.

materials. The properties of continuous fiber reinforced composites can be controlled by volume fraction of fibers.

Few works reported about the printing of continuous fiber reinforced composites using two separate print heads. The matrix material (in the filament form) has been printed in one stage and reinforcement material in another stage [19]. This process schematic is shown in Fig. 2b. Initially, the fiber bundle will be printed with *concentric* or *isotropic* pattern, and then the matrix will be printed in the gaps before the next layer of fiber printing. As can be seen from Fig. 2c, in the concentric pattern, fiber printing starts at the outer edge and wraps towards the center and the isotropic pattern consists of parallel lines. It should be noted that the fiber should be stiff enough to print in concentric and isotropic patterns. Markforged® has further developed and commercialized these printers with separate supply spools for both continuous fiber and thermoplastic filaments [27]. However, these printers are mostly limited to print only nylon as matrix material and printing using other thermoplastic material is difficult. To improve the adhesion of the reinforcement to the nylon matrix, the reinforcing fiber filaments are also coated with a nylon material. In general, the design of printing using two separate heads offers advantages of selecting and customizing different combinations of fibers and polymers. In addition to that, the fiber volume fraction in the individual deposited layer can be controlled.

There are still some challenges that need to be resolved in FDM of composite materials. The critical requirement for any material to be used in FDM is that it can be processed into a feedstock filament. Most of the commercial printers require a filament of 1.75 mm diameter as the feedstock material. Making this filament of constant cross sectional diameter is quite challenging, especially for the particle or short fiber reinforcements. The composite material that needs to be printed should possess sufficient melt viscosity, strength, modulus and ductility. In the liquefier head, the filament forces the upcoming material out of the nozzle. If the filament has high viscosity and low stiffness, filament buckling will occur. It is desired to have a less viscosity and high strength for the filament. The flow of reinforcements in the nozzle and the pressure drop required for extruding the material through the nozzle highly depend on the melt viscosity. Venataraman et al. proposed an index for printability as the ratio of the elastic modulus to the melt viscosity. It is reported that if this ratio is higher than a critical value (3.5×10^5) will not cause buckling [28]. The addition of fillers tends to

increase the viscosity by several orders. Often, to reduce the viscosity with the addition of reinforcements, other additives such as surfactants and plasticizers need to be added, making the process even more challenging. The addition of fillers cause the agglomerate formation, blockage of printer heads and improper adhesion during printing.

The final properties of the printed parts are difficult to control because several process parameters effects the process [29,30]. As shown in Fig. 3, these parameters can be categorized as.

1.2. Material parameters

- Polymer type: Amorphous or semi-crystalline nature of the polymer and their crystallization temperatures. (The FDM process is highly suitable for printing amorphous polymers because they quickly solidify with less degree of shrinkage. This behavior of the printed layer is essential to stick to the upcoming layer. The solidification of semi-crystalline polymers may take longer time depending the degree of crystallinity and the cooling rate. The crystalline nature also causes a high degree of shrinkage and part distortion.)
- Filler type: Discontinuous (Particles, short fibers) and continuous fibers
- Filler morphology: Size and shape of discontinuous reinforcement

1.3. Machine and print parameters

- Build Orientation: It refers to the inclination of the part in a build platform with respect to X, Y, Z axis. X and Y-axis are considered parallel to build platform and Z-axis is along the direction of part build.
- Raster angle: Direction of the raster relative to the X-axis of build table.
- Layer thickness: It refers to the thickness of the deposited layer.
- Nozzle diameter: It depends upon the type of nozzle used. Commercial printers mostly use 0.4 mm nozzle diameter. During the printing of short fiber or particle reinforced composites, the agglomeration of reinforcements yields nozzle blockage. For composite material printing, generally high nozzle diameters are recommended.

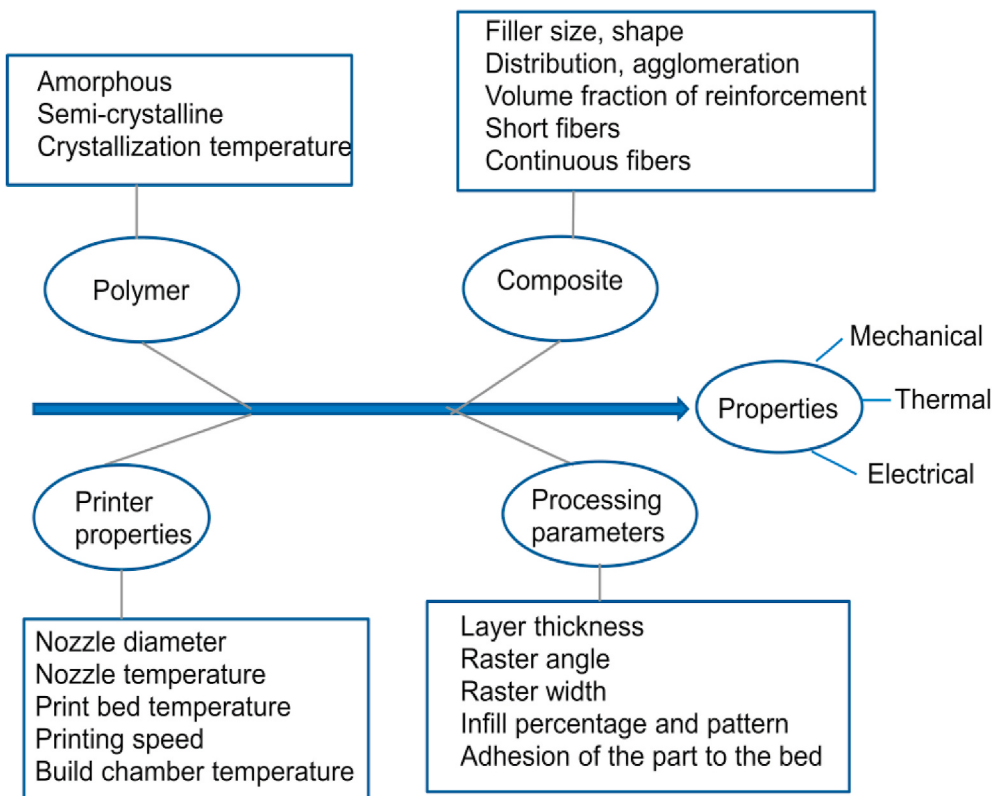


Fig. 3. Different parameters that affect the properties of FDM printed parts.

- Raster width: Width of raster pattern used to fill interior regions of the part.
- Number of contours: The number of contours of the part outside
- Raster to raster gap (air gap): It is the gap between two adjacent rasters in a same layer. Negative air gap refers to the overlap of rasters. Positive air gap allows space between rasters. Printing with zero air gap is highly recommended.
- Infill density: The amount of material that is used to build the part inside. For example; the inner layers of the part can be printed in hexagonal or rectangular pattern.

Few review papers are available in the literature, which gives an overview of 3D printing of composite materials. These reviews briefly explain about different printing techniques such as Selective Laser Sintering (SLS), Stereolithography (SLA), Ink jet printing etc. [20,31–37]. Among these techniques, FDM is a simple and cost effective process. Therefore, most research works focused on expanding the capability of FDM to print different composite material systems [38–41]. The available reviews on FDM of composites concentrated only on few aspects such as FDM of carbon fiber reinforcements [39], natural fiber reinforcements [40], PLA composites [41] and composite printing for tooling applications [9]. Given the importance of FDM, a thorough review of the past work is needed for different composite materials ranging from amorphous to crystalline and intermediate to high temperature polymers. The present paper gives an in depth analysis of the FDM of acrylonitrile-butadiene-styrene (ABS), polylactic acid (PLA), polyamide, polypropylene (PP), polyethylene (PE), polyethylene terephthalate glycol (PETG), polyether-ether-ketone (PEEK), polyetherimide (PEI), polyphenylenesulfide (PPS), polycarbonate (PC), polycaprolactone (PCL) and thermoplastic elastomers (TPE). The effect of all types of reinforcements ranging from powders to continuous fibers is discussed. Finally, this review explains the application of FDM printed composite parts in biomedical, electrical, functional and aerospace applications. The use of mathematical modeling for simulating the printing

process and models for estimating the mechanical properties of the composite printed parts is also highlighted. The present paper may serve as a primary reference for young researchers.

2. FDM of thermoplastic composites

Major issues during the FDM printing are the presence of void content in the microstructure, dimensional inaccuracy and the anisotropy of the printed parts. They arise due to the weak intra layer bonding between beads in a single layer and weak inter layer bonding between different layers in the thickness direction. Therefore, the strength of printed parts is limited. All research work in the area of layer wise additive manufacturing mainly focus on overcoming one or two of these problems. Even though polymer composites exhibit higher mechanical properties than polymers, properties of composite printed parts are still inferior. This is due to presence of weak reinforcement/polymer interface in case of continuous fiber reinforced composites and poor interface stress transfer in case of short fiber or particle reinforced composites. Particularly, the processing route of nano composites has major effect on the interface strength. In this review, discussion is mainly focused on void content, anisotropy and interface strength of the parts made via FDM of thermoplastic composites.

2.1. FDM of ABS composites

ABS is a widely used thermoplastic material in FDM because it has sufficient melt fluidity, desirable stiffness and strength. The tensile, compressive and flexure strength of FDM parts made of ABS are low compared to the parts fabricated by injection molding. For instance, FDM fabricated ABS has only 74% tensile strength to that of injection molded ABS [42]. This is due to high material compaction in the injection molding process. Also, in FDM, layer by layer addition induces anisotropy in the built part. Ahn et al. conducted a series of experiments to investigate the effect of different process parameters on the

anisotropy and strength of ABS printed parts [42]. The negative air gap and raster orientation has a major influence on mechanical properties. Dawoud et al. reported that providing a negative raster gap will result in high packing of the material and hence properties are improved [43]. To improve mechanical properties and mitigate the print orientation induced anisotropy, several studies have been performed to print ABS composites. Zhong et al. conducted experiments to investigate the processability of short glass fibers reinforced ABS matrix composites. The addition of glass fibers decreases the ductility. The filament could not be wounded into the spool after extrusion due to brittle nature of the composite. Addition of plasticizer makes the composite ductile and filaments of constant diameter can be prepared [44].

Carbon based reinforcements improve the mechanical and electrical properties of polymers. Shofner et al. developed ABS matrix composites by reinforcing vapour grown carbon fibres (VGCF) and single-walled carbon nanotubes (SWNT) [45]. Tensile tests have been conducted on three different specimens: thin sheets of composites, extruded composite filaments and on the parts made of extrusion freeform fabrication. Both of these nanofillers dispersed homogeneously in ABS and the composites showed an increase in strength and modulus. During the filament extrusion, reinforcements are aligned along the extrusion direction. The extruded fiber showed an increase in strength and modulus compared to the composites. Despite preferred orientation in the filaments, the strength of the printed parts showed decrease in strength and modulus due to voids. Compared with unfilled ABS printed parts, nearly 40% and 60% increase in tensile strength and tensile modulus were obtained at nanofiber loading of 10 wt% [46].

Ning et al. reinforced short carbon fibers of 7.2 μm diameter and 100 μm length in the ABS [47]. The improvement in tensile strength and elastic modulus of the printed parts is observed at 5% and 7.5%, respectively. As shown in Fig. 4a, three types of voids have been reported in this study. Pore type 1 is due to gas evolution. Pore type 2 is the inter layer void and pore type 3 is the void at the interface between fiber and matrix with the bead. It is also reported that the increase in the length of carbon fibers increases the strength and modulus but decreases the toughness and ductility. Tekinalp et al. processed short carbon fiber (0.35 mm length) reinforced ABS composites and reported an increase of 115% in tensile strength and 700% increase in modulus of the printed parts [23]. An important observation has been reported about the voids in the printed parts. Triangular shaped voids are formed between the beads in the printed parts and the void size is reduced compared to the pure ABS printed parts. However, with the addition of short fibers, additional voids have also been observed within the beads due to the poor interface between carbon fibers and ABS (refer Fig. 4b and c). Up to 30 wt % of carbon fiber loading, a great improvement in strength and modulus has been observed, but nozzle clogging was observed for higher loadings. Zhang et al. processed FDM parts using carbon nanotube reinforced ABS and carbon fiber reinforced ABS composites. It is observed that the strength and modulus of printed parts is higher for these two composite material systems, though the void content in the printed parts is higher compared to pure ABS printed parts. Also, the

carbon nanotube reinforced ABS printed parts showed less void content than the carbon fiber reinforced ABS [48]. Printing at a less layer thickness of 0.8 mm, low printing speed of 60 mm/s and 0° degree raster orientation showed the highest properties. Love et al. investigated anisotropy of ABS + short CF composite 3D printing [49]. It is reported that the composite print parts showed anisotropy. The tensile properties of specimen printed along longitudinal direction are higher than the properties of the specimen built vertically. Also, it is reported that the addition of short carbon fibers increases thermal conductivity and increases thermal expansion coefficient which are key to the dimensional stability of the printed parts. Weng et al. prepared nanocomposites by reinforcing organically modified montmorillonite (OMMT) by melt intercalation [50]. The addition of 5 wt% of OMMT significantly improved both tensile and flexural strength and modulus of the printed parts.

The new generation material graphene attracted most attention recently, which will improve the properties when reinforced with polymers [51,52]. However, the dispersion of graphene may not be good in majority of polymers. The graphene oxide (GO) has better dispersion ability, however, the electrical properties will be decreased because of the presence of sp^3 bonds in GO. Reducing GO in reductants such as Hydrazine restores sp^2 bonds and improves the electrical properties. Wei et al. processed graphene oxide (GO) reinforced ABS composites using the solvent method for different weight fractions. The two solutions, GO sheets in NMP and ABS in NMP were mixed using homogenizer and this mixture was later reduced in Hydrazine. Filaments of Graphene-ABS composites are prepared using a single screw extruder and used for FDM printing [53]. It is demonstrated that the graphene nanocomposites with up to 5.4 wt % graphene are 3D printable and beyond this graphene loading, the nozzle blockage occurs. The printed parts showed enhanced electrical conductivity properties than pure ABS parts. The selection of a proper solvent for the components to dissolve initially and remove the solvent from the composite is challenging. Dul et al. processed graphene nanoplatelets (GNP)-ABS composites using melt compounding (dry mixing) [54]. The GNPs were added to the ABS melt and mixed using the counter-rotating extruder. It is observed that the elastic modulus increases with graphene loading, but tensile strength and elongation to breakage decreases. Also, at filler loadings higher than 4 wt%, nozzle block is observed during printing. The size of the reinforcement is the key issue as higher size particles may block the nozzle. Aumnate et al. compared the GO/graphene composites prepared using both the solvent and melt compounding methods [55]. It is reported that the size of fillers are in the order of 10 μm and 3 μm for dry mixing and solvent mixing routes, respectively. The GO/ABS filament made from the dry mixing failed to print due to the agglomeration of GO and die clogging.

In addition to the carbon based materials, a significant increase in thermal and mechanical properties is also observed by the addition of metal powders. Nikzad et al. reinforced metal fillers such as iron and copper up to 40 wt% in ABS and found a significant increase in stiffness of the printed parts [56]. The reinforcement of metal fillers may increase the viscosity of the composite. Therefore, additives such as surfactant

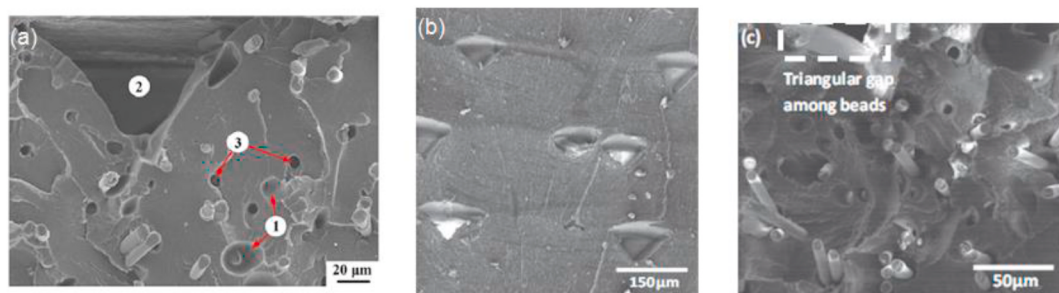


Fig. 4. The presence of voids in the FDM printed composite parts a) ABS+10 wt.% short carbon fibers of 150 μm length [47] b) neat ABS c) ABS+10 wt % short carbon fibers of 0.35 mm length [23] [Reprinted with permission].

and plasticizers needs to be added. The injection molding tools printed using metal-ABS composite showed better stiffness than the tools made of pure polymeric materials. Ryder et al. processed ABS-stainless steel composites [57]. Initially, the ABS has been dissolved in acetone and stainless steel powder has been added to this mixture. A reasonably good uniform distribution of powder particles has been observed. It is reported that beyond 14 wt.% of metal addition, enhancement of mechanical properties is not observed. Torrado et al. investigated the effect of different additives such as Jute fibers, TiO_2 , ZnO , SrTiO_3 , Al_2O_3 [58, 59]. Printing process of ABS: styrene ethylene butadiene styrene (SEBS) and ABS: ultra high molecular weight polyethylene (UHMWPE) polymer blends is also explained. Fig. 5 shows the microstructure of the failed samples of FDM printed ABS-Jute, ABS- TiO_2 and ABS:SEBS polymer blend. In the case of Jute fiber composites, additional micro voids are observed in the filament itself due to the decomposition of Jute under processing temperature. The printing of ABS-metal oxide powder does not improve any inter layer adhesion but micro voids in the printed beads are reduced. The improved adhesion and ductile fracture mode is observed in case of blends. It is reported that the printed specimens made using ternary blends showed a decrease in anisotropy. The ultimate strength values for the longitudinal and vertical prints are approximately 15 MPa and 12 MPa respectively. However, this value is lower than the ultimate strength of ABS parts. The improvement in anisotropy is observed at the expense of a decrease in ultimate strength.

Boron nitride (BN) is becoming a promising material to reinforce with polymers that can be used in thermally conductive but electrically insulating applications. Quill et al. reinforced boron nitride in ABS and observed an increase in thermal conductivity about 5 times to ABS [60]. The agglomeration of BN and voids in the FDM printed parts causes the decrease in flexural and impact properties. Even though the mechanical properties are reduced, boron nitride shows much advantage in thermally conductive applications. Hwang et al. processed ABS-Cu and ABS-Fe composites by dry mixing and these pellets are further extruded into filament [61]. The FDM printed parts showed an increase in modulus and decrease in strength for both fillers. However, the thermal conductivity of the printed parts has been increased for with the addition of Cu. Khatri et al. reported that the relative permittivity of ABS-barium titanate composites increases non linearly with BaTiO_3 loading but at loadings higher than 35 vol %, the feedstock filament cannot be processed due to filament breakage [62]. Osman et al. prepared ABS -rice straw composite filaments for FDM [63]. The addition of rice straw increases the porosity in printed parts and the strength of the parts decreased. These parts can be used for low load level applications by effectively using the naturally available rice straw.

2.2. FDM of PLA composites

PLA is another common thermoplastic material used in FDM, which has wide applications in the medical industry due to its biodegradable/biocompatible properties. It has a lower ductility than ABS but has higher strength [64]. Similar to FDM of ABS composites, an increase in void content and the anisotropy is observed during the printing of PLA

composites. For example, Ferreira et al. processed FDM parts using PLA and chopped short carbon fiber (60 μm length) reinforced PLA. The fibers were observed to be aligned along the filament's length during extrusion and are aligned along the print direction during printing. It is observed that tensile and shear modulus of the composite printed parts are higher than about 100% compared to pure PLA printed parts [65]. The failure strain of PLA + carbon fiber composite is lesser than PLA because the composite became more brittle after adding short carbon fibers. Also, there is not much change in tensile strength is observed with the addition of carbon fibers. The reinforcement of carbon fibers in PLA results in a weak bonding interface due to the poor adhesion of reinforcements. If the length of reinforcement is increased, good adhesion may be observed because of the increase in the external surface area. While increasing fiber length enhances the adhesion in ABS composites, PLA composites show poor adhesion for longer fiber lengths.

Investigations have been carried out to find the effect of other carbon derivatives such as carbon nanotubes and graphene on PLA. Plymill et al. prepared nanocomposites by reinforcing graphene and multi-walled carbon nano tubes (MWCNT) individually using twin screw extruder, which provides a high shear rate mixing [66]. The resulting composite in pelletized form is fed into a single screw extruder for preparing the FDM feedstock filament. Filaments of constant diameter have been prepared by proper control of the cooling rate at the nozzle exit. An increase in the tensile strength of the printed parts has been observed at 0.2 wt% loading of graphene and 0.1 wt% loading of MWCNT. Bustillos et al. printed FDM parts from the commercially available conductive PLA-graphene filament from BlackMagic © [67]. Fig. 6 compares the microstructure of the PLA and PLA-graphene printed parts. The inter layer adhesion is much stronger in PLA and voids are observed between the layers during the printing of composite. The PLA-graphene composite filament experiences a high cooling rate because of high thermal conductivity of graphene. This creates a strain mismatch between fiber and matrix leading to a weak inter layer bonding. Caminero et al. printed FDM parts using commercially available graphene filament from Haydale Ltd.© [68]. It is reported that the addition of graphene nanoplatelets increases tensile and flexural strength but decreases the impact strength. The anisotropy of the printed samples has been investigated by printing the specimens along flat, on-edge and upright positions. The tensile, flexural and impact strength has been decreased by almost 30% for an upright position. Also, it is reported that the presence of graphene nanoplatelets increases the surface texture without effecting the geometrical dimensional accuracy.

The weak strength along the transverse direction of the printed parts is attributed to the poor inter layer adhesion of polymers. The adhesion is stronger if the polymer surface is heated above its sintering temperature. However, during the FDM process, the cooling is faster because of the short times involved, and hence the inter layer adhesion is weaker. To avoid this problem, trials have been made to increase the heating time using air nozzles. However, this process resulted in the high dimensional inaccuracy of printed parts. An interesting study has been presented by Sweeney et al. to increase the interlayer strength by local heating of polymer interfaces [69]. In this work, the PLA filament is

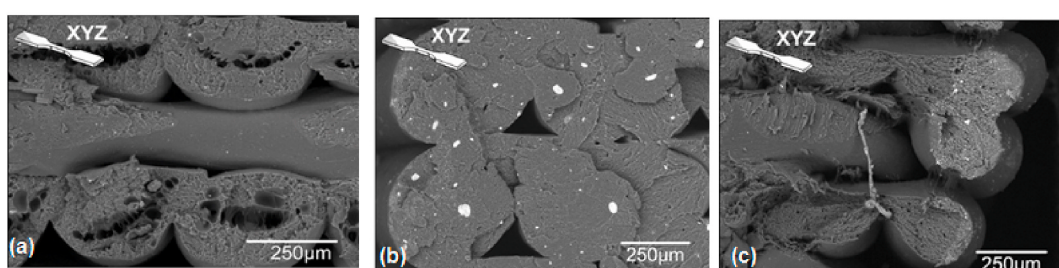


Fig. 5. The microstructure of the failed specimens of FDM printed a) ABS + Jute composite, b) ABS+ 5 wt % TiO_2 particle composite c) ABS:SEBS polymer blend [59] [Reprinted with permission].

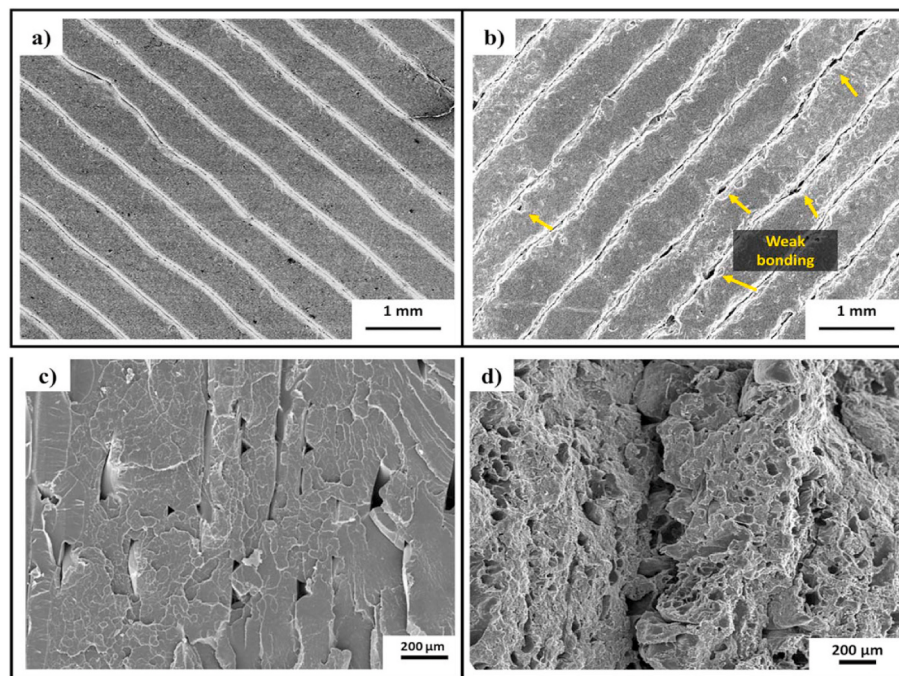


Fig. 6. Microstructure of 3D printed (a) PLA and (b) PLA-graphene parts. Fractured cross-sectional. Microstructure of 3D printed (c) PLA and (d) PLA-graphene [67]. [Reprinted with permission].

coated with CNTs before printing (refer Fig. 7). During the printing process, the localized heating at nano scale using microwaves causes the surfaces to melt and promotes inter layer adhesion. The study reported an increase in fracture strength by 275% with this local welding by microwave heating. Further, Ivanpy et al. Reported that the addition of bifillers (both CNT and Graphene) increase electrical properties and reduce agglomeration [70]. PLA printed parts also has excellent bio compatibility as explained later in the section on applications of FDM [71–73].

In continuous fiber reinforced composites, the poor adhesion between matrix and fiber interface deteriorates mechanical properties. Matsuzaki et al. processed continuous carbon fiber reinforced thermoplastic (CCFRTP) composites using continuous carbon fiber tows and jute twisted yarns as reinforcements in PLA and these composites have been 3D printed [24]. The study reported that the tensile strength and modulus of CCFRTP composite printed parts are higher than the part properties using other composite printing techniques such as selective laser sintering (SLS). These mechanical properties are also higher than the FDM printed parts using short carbon fiber reinforced composites. It is also reported that mechanical properties of these parts can be further

increased by increasing the volume fraction of continuous fibers. However, poor adhesion between the matrix and fiber has been observed. In general, the surface treatment of fibers enhances the mechanical properties of composites. Li et al. processed CCFRTP printed parts after applying the PLA compatible sizing agent such as methylene dichloride [74]. As shown in Fig. 8, the fiber-matrix interface adhesion is improved in the printed parts. The resulting 3D printed parts showed an improved tensile and flexural strength compared to PLA and unmodified composite. Tian et al. studied FDM process parameters such as liquefier temperature, layer thickness on the interface and performance of the continuous fiber 3D printed structures [75]. The study also showed the capability of the FDM process for printing large curvature products using CCFRTP. In another study, Tian et al. recycled the FDM printed continuous fiber reinforced PLA composites and the resulting materials were again 3D printed [76]. The parts made of recycled composite showed a better tensile and flexural properties because the residual impregnation of PLA improved the fibre-matrix adhesion.

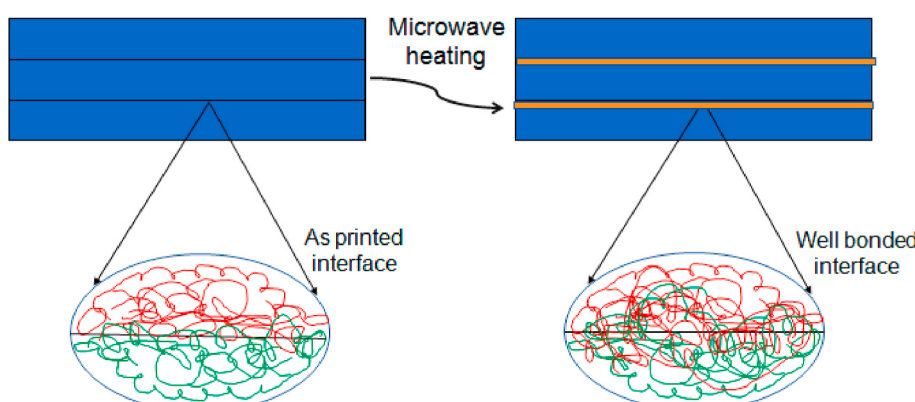


Fig. 7. The interface is locally heated to allow for polymer diffusion and increased fracture strength [69].

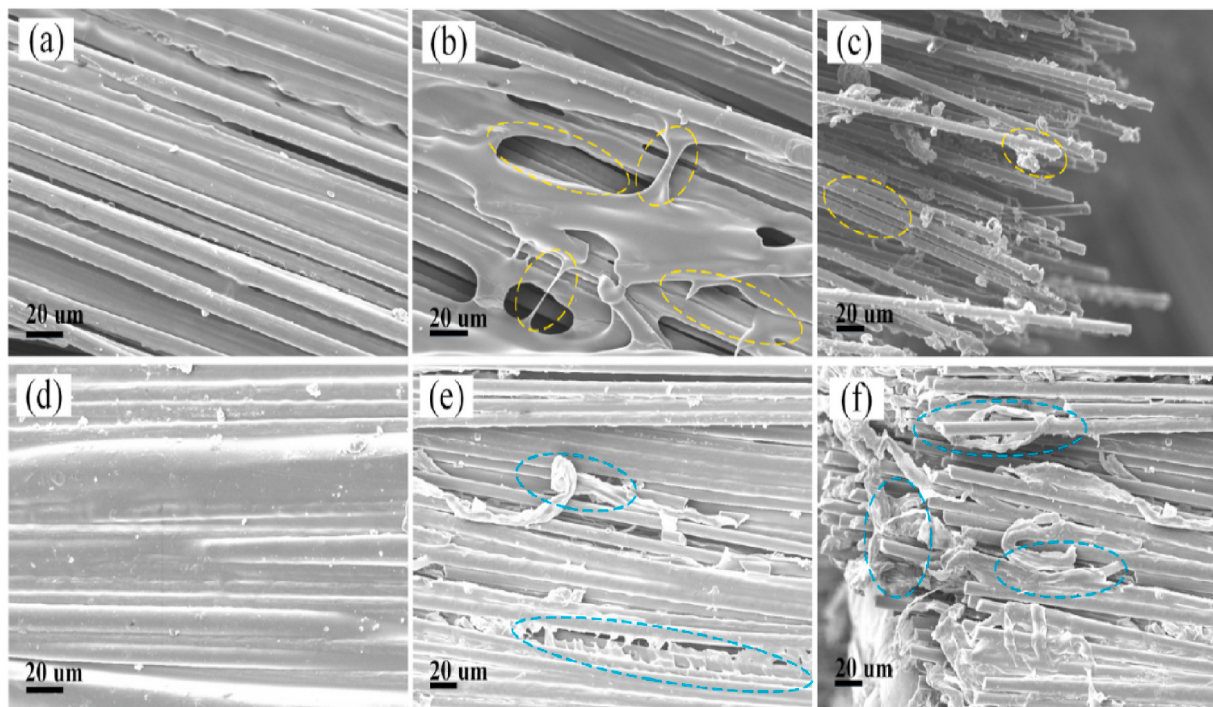


Fig. 8. a) Thermoplastic PLA filament coated with CNT-rich layer b)After the microwave heating, the interface is locally heated to allow for polymer diffusion and increased fracture strength [74]. [Reprinted with permission].

2.3. FDM of nylon/polyamide

Nylon has properties similar to that of commercial ABS and can be processed into feedstock filament at a low cost [6,77]. Particle reinforced nylon composites have been used to print molds for tooling applications. Masood et al. manufactured injection molding inserts through the FDM of nylon + iron metal powder composites [6,77]. The iron metal powder has good mechanical and thermal properties and a high amount of mixing and surface binding with polymers. Small quantities of plasticizer and surfactants are added to improve the flow, dispersion and toughness properties of the composite. The land length of the die was increased from 5 to 10 mm to avoid a phenomenon known as die swell, which is primarily due to the elastic recovery of the metal-polymer composite in the die. The processed injection molding inserts have desirable mechanical properties. It is reported that the size and volume fraction of the filler has a significant influence on the mechanical properties. Large size fillers increase tensile modulus and small fillers increase the tensile elongation [78]. Singh et al. processed Al₂O₃ reinforced nylon matrix composites to develop wear resistant materials for grinding applications with special applications in the dentistry. The amount of filler and its size are chosen appropriately, such that the melt flow index (MFI) of the processed composite is equal to MFI of ABS. The wear tests on the FDM prepared parts using these composites revealed the wear resistance of this composite higher than the Al₂O₃ –ABS composite [79–81]. Further, the authors performed experiments to investigate the effect of particle size. Nylon composite FDM feed stock filaments have been prepared using single particles and a mixture of two and three particles of different diameters. The particle size of more than 150 μm may cause nozzle clogging and the size of all fillers used is less than that in all cases. MFI of all mixtures is near to commercial ABS material (2.41 g/10 min).

Abdullah et al. processed zirconium oxide filled nylon composites to use in FDM for printing patient specific implants [82]. At higher loadings and for the particle size of 400 μm, agglomeration of particles occurred in the composite and this caused the nozzle blocking during 3D printing by a 0.4 mm nozzle. Due to this, the properties of the printed

parts are reduced compared to the properties of pure polyamide printed parts [82]. Zhu et al. prepared composites of polyamide 12 with 6 wt% of graphene nanoplatelets (GNP) in pellet form by melt compounding using twin-screw extruder [83]. FDM filaments are prepared by single screw extruder from these pellets. It is reported that the 6 wt% of graphene loading enhanced the thermal conductivity and elastic modulus of 3D printed parts by 50% and 7%, respectively. The scanning electron microscope (SEM) images of the failure of 3D printed samples showed that the GNPs are highly oriented along the print direction during the nozzle extrusion. The authors did not report the nozzle blocking issues at this high loading of GNPs. The addition of GNPs increases the melt viscosity, which effects the coalescence. The sintering behavior and coalescence rate can be described using

$$X = \left(\frac{\Gamma t}{\mu a} \right)^{0.5}$$

where X is the coalescence rate, t is the sintering time, Γ is the surface tension, a is particle radius and μ is the viscosity. As the viscosity increases because of the addition of GNPs, the coalescence during PLA/graphene composite is lesser. Due to this, triangular shaped voids have been observed.

Currently, nylon is mostly used as the matrix material for commercially available continuous fiber reinforced printers. To increase the adhesion of fibers to the nylon matrix, fibers are also pre-impregnated with nylon. For instance, nylon impregnated glass and carbon fibers are commercially available. The in-situ fusion in the in-nozzle impregnation technique can be useful for controlling the fiber volume fraction, however weak matrix and fiber interface remains a challenge. The printing using the pre-impregnated continuous fiber may have a better interface, but the amount of volume fraction of fibers is limited.

Goh et al. processed continuous fiber-reinforced thermoplastic carbon and glass composites (CFRTP and GFRTP) using FFF [84]. Nylon matrix pre-impregnated fiber filaments are used as feed stock. The authors carried out tensile, flexural, and indentation tests and the failure mechanisms in each mode have been analyzed. As shown in Fig. 9, tensile rupture perpendicular to loading direction and shear damage

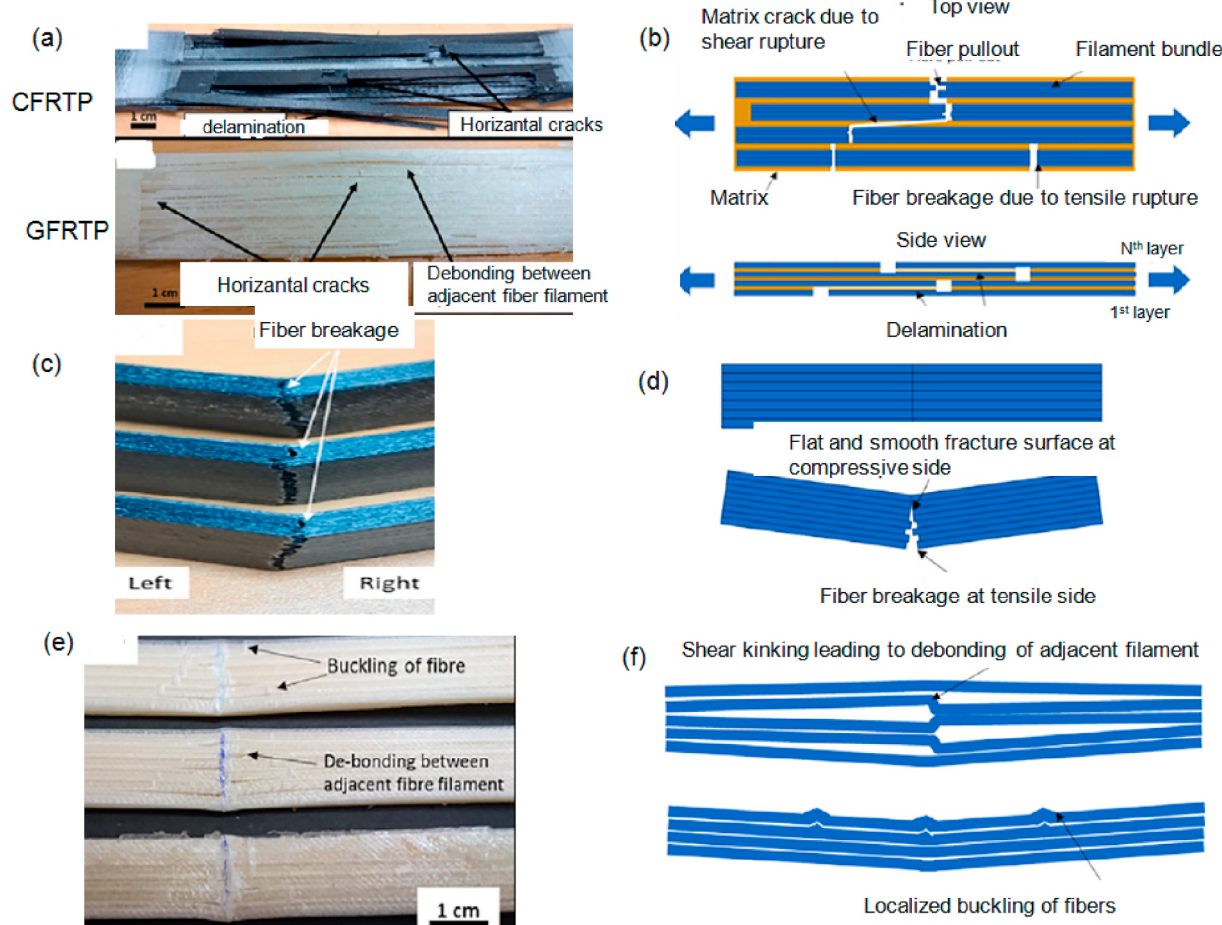


Fig. 9. Illustration of the failure mechanism of 3D printed continuous fiber reinforced composites, Tensile behavior: a) and b), Flexure behavior of Carbon FRTP: c) and d), Flexure behavior of Glass FRTP: e) and f), [84]. [Reprinted with permission].

along the fiber direction is observed as the main failure mechanism in tensile tests. Delamination and debonding between the adjacent fiber filaments have also been observed. In the bending tests, cracks initiated at the peak compression place in CFRTP and propagated towards the neutral plane due to lower compressive strength of carbon fibers. Catastrophic failure occurs when the tensile side stress reaches its peak value. No crack observed in GFRTP specimens, rather buckling of fibers is observed due to shear kinking and matrix failure. In the indentation tests, debonding between adjacent filaments, delamination and fiber breakage has been observed as the main failure mechanisms.

Dickson et al. processed continuous fiber reinforced composites using two separate print heads in which nylon was printed in one stage and reinforcement in another stage [85]. Initially, the fiber bundle will be printed with a *concentric* or *isotropic* pattern, and then the nylon matrix will be printed in the gaps before the next layer of fiber printing. Continuous glass, carbon and Kevlar individual fiber reinforced nylon matrix composites have been printed. It is reported that the isotropic pattern yields excellent properties in tension and concentric pattern yields better properties on bending. It is also reported that with an increase in fiber volume fraction, the strength of continuous fiber reinforced composites increases. For example, the tensile strength of 33 vol % of glass fibers printed in a concentric pattern matches the strength of aerospace grade aluminum [85]. This example highlights the potential of FDM to print parts for real time applications with control of the fiber volume fraction. However, as the fiber content increases, the void percentage also increases thus limiting the maximum fiber volume fraction.

Melenka et al. investigated the effect of fiber volume fraction on mechanical properties in the continuous fiber reinforced structures [86].

In this study, continuous Kevlar fiber is printed in the form of concentric rings in the thermoplastic matrix. A comparative study has been presented with pure nylon, and nylon with two, four and five concentric rings. The increase in the number of concentric rings represents the increase in volume fraction of fibers and enhances the mechanical properties of the printed parts. Elastic modulus and ultimate tensile strength increase linearly with fiber volume fraction. Al Abadi et al. analyzed the effect of volume fraction and fiber orientation on the structural performance of the 3D printed composites using the combination of analytical and experimental results [87]. The test specimens were printed with individual glass, carbon and Kevlar fibers. Both glass and Kevlar fibers were printed in biaxial (0/90) and carbon fibers were printed using concentric rings. Because of the high stiffness of the carbon filament, biaxial printing is difficult. It is reported that the elastic properties are dependent on the volume fraction of the fiber for all composite printed parts.

2.4. FDM of polypropylene

Polypropylene (PP) is a semi-crystalline polymer that is extensively used in packaging, household furniture, medical and automobile applications. It is a promising thermoplastic material with its high impact strength and low cost. Parts made of it possess dimensional inaccuracies because of the high thermal expansion and warping nature. Carnerio et al. demonstrated that the semi crystalline nature of PP causes shrinkage of the printed parts leading to distortion and decoupling from the print bed, as shown in Fig. 10 a [88]. Maintaining the nozzle temperature at 165 °C and printing the initial layer (that is in contact with

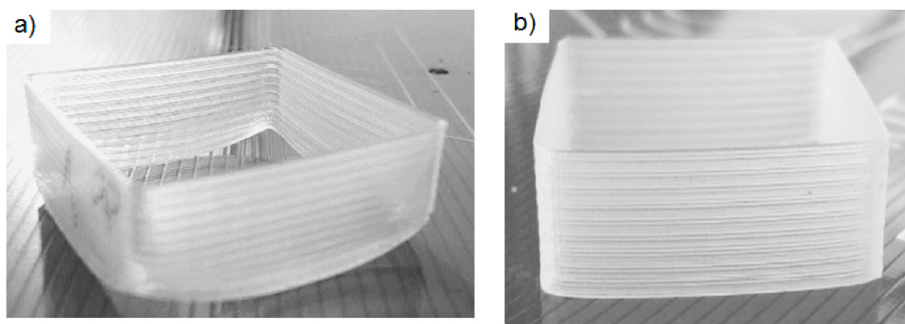


Fig. 10. FDM printed polypropylene a) with distortion and decoupling from the bed, b) reduced distortion and improved adhesion to the bed at optimal printing parameters [88]. [Reprinted with permission].

the bed) at very low printing speed, and printing with an optimum unidirectional orientation drastically reduced the warpage (Fig. 10 b). It is to be noted that the adhesion of polypropylene to the regular print surfaces is very poor. Changing the print surface to an adequately cleaned polypropylene plate promotes the adhesion. Other studies on FDM printing using PP reported that the shrinkage and warpage could be reduced by adding fillers and controlling the build chamber temperature. Spoerl et al. [89–91] processed PP composites with expanded-perlite fillers and found that the addition of small size fillers results in the reduction of shrinkage and warpage. The small sized fillers enhance the filler-matrix adhesion, reduce the polymer chain orientation and constrain the polymer from shrinking. An increase in the build chamber temperature alters the morphology of the crystal growth. For example, maintaining the chamber temperature at 55 °C resulted in spherulites formation, which causes a decrease in the warpage. However, the addition of fillers decreases the impact strength. The effect of build chamber temperature on the crystal growth and mechanical property enhancement needs to be further investigated.

Carneiro et al. prepared glass fiber reinforced PP composites, whose modulus and strength are higher than PP by 30% and 40%, respectively [88]. The FDM feed stock filament prepared from glass-fiber PP composites maintained the minimum critical length after the extrusion. However, the properties of the 3D printed glass PP composites are still lesser compared to the parts made of compression molding. Stoop et al. explored the possibility of using the recycled PP for FDM [92]. Composites are made by reinforcing harakeke, hemp fibers and gypsum powders in the recycled PP. The composites are initially prepared by blending PP and reinforcements in a twin-screw extruder. For the natural fiber reinforcements, beyond 30 wt% of hemp and harakeke fibers, the dimensional accuracy of the filament is not properly maintained and a ‘Sharkskin’ effect has been observed on filaments. However, there is no such effect was observed with the addition of gypsum powder. It is reported that while the natural fiber reinforcement increases the stiffness and strength of filaments, the mechanical properties of 3D printed parts decreased possibly due to the formation and voids and stress relaxation of the polymer occurring during 3D printing. However, the 3D printed parts with natural fiber reinforcement showed a decrease in the distortion. For instance, the addition of 30 wt%. Natural hemp fiber reduces the part distortion significantly, as shown in Fig. 11.

2.5. FDM of polyethylene

Polyethylene (PE) is a commonly used thermoplastic polymer in daily life. PE polymers are categorized as low density polyethylene (LDPE), high density polyethylene (HDPE), ultra high molecular weight polyethylene (UHMWPE), etc. PE polymers have excellent recyclability and are potential materials for sustainable manufacturing [93]. The processing of PE via FDM adds a new dimension to the additive manufacturing technology due to recyclability of parts. However, PE has the highest volume shrinkage rate upon solidification, a high degree of



Fig. 11. a) Shrinkage of the FDM printed polypropylene part b) Reduction in shrinkage of PP with 30 wt%. Natural fiber hemp [92]. [Reprinted with permission].

warpage and does not easily stick to the print platform. Similar to PP (as shown in Fig. 10), the adhesion to the print platform can be enhanced and the warpage of the printed part can be decreased by selecting optimal print and process parameters. Schirmeister et al. suggested that using SEBS (styrene-block-ethene-co-butene-block-styrene) as a support material showed better adhesion for HDPE printing [94]. The part can be easily detached from the built platform with excellent surface quality. The same study also reported that providing a gradient in the filling amount can greatly reduce the void content in the printed parts. For example, filling 100% in the first layer and 107% in the sixth layer significantly reduced the void content, refer Fig. 12. Because of the reduction in void content, the mechanical properties of the printed parts with this optimal print parameters are almost equal to the properties of the injection molded (IM) HDPE. The study reported that the elongation to break is less when compared to IM specimens. However, this property can also be increased by optimizing the process parameters.

Additions of high performance filler materials to PE and printing of these composite materials can extend the applicability of FDM. Bedi et al. processed PE/Al₂O₃ composites with different Al₂O₃ particle size [95]. The thermoplastic granules collected from house hold waste like plastic films, package bags etc. are blended with Al₂O₃ particles and the composite filaments are prepared using twin screw extruder. The MFI is decreased for the composite compared to PE. The composite filaments are used to print prototypes for rapid tooling. The printed molds showed better wear resistant performance and are thermally stable. Olesik et al. demonstrated the FDM printing using LDPE composites using finely powdered glass [96]. The addition of glass powder reinforcement improved the wear resistance by 50% and the printed parts are potential candidates for low-duty frictional applications. Tarres et al. processed biocomposites using thermomechanical pulp (TMP) as the reinforcement in HDPE [97]. The study reported that the printing of neat HDPE failed due to improper adhesion. The adhesion is improved for the composite by adding the compatibilizer such as maleic anhydride functionalized polyethylene. The mechanical properties of the printed

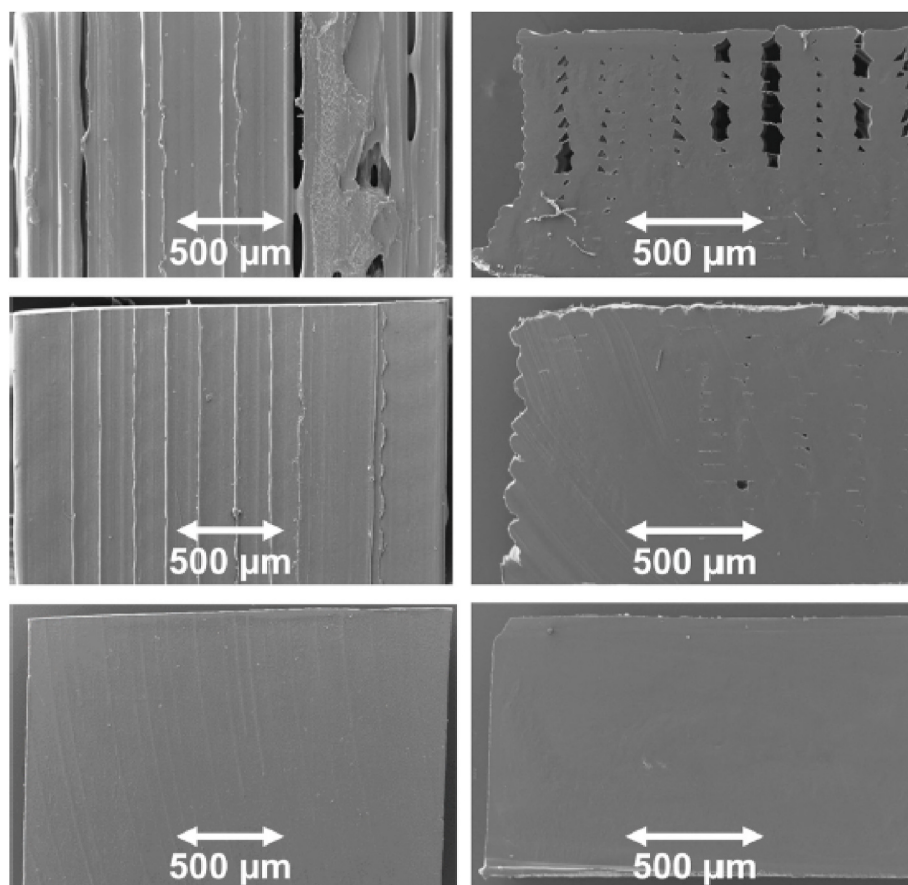


Fig. 12. SEM images of the surface (left) and cross sectional area (right) of HDPE specimens obtained by FFF (1–4) and by injection molding, respectively (5–6). In contrast to regular printing (1 and 2) FFF with gradually adjusted filling amount (3–4) is clearly superior in terms surface quality and preventing defect formation [94]. [Reproduced with permission].

composites are improved.

Polyethylene terephthalate glycol copolymer (PETG) is used in food and medical applications. It has high chemical and impact resistance along with excellent recyclability, biocompatibility. The crystallinity of this polymer is very low (only up to 3%). Therefore, it is very much suitable for extrusion printing. However, parts printed with PETG contain high porosity. For example, 19% porosity has been reported in Ref. [98]. The elastic modulus, tensile strength and elongation to break of printed parts are much less compared to bulk PETG filament. Few works reported an increase in mechanical properties with glass fiber [99] and CNT reinforcement [100]. Other works reported an increase flexure strength [101] and a decrease in porosity of printed parts with short carbon fiber reinforcement. Guessasma et al. suggested that printing at nozzle temperature of 250 °C increases the tensile strength of unreinforced parts [98]. This study reported that, optimizing the process parameters such as nozzle temperature has much more positive effect than reinforcing the polymer with fillers.

2.6. FDM of polyether ether ketone (PEEK)

Poly-ether-ether-ketone (PEEK) is an interesting semi-crystalline high performance thermoplastic polymer with a molecular structure presenting aromatic groups and both ether and ketone group in the backbone. PEEK has superior properties (T_g between 143 and 148 °C, T_m between 330 °C and 340 °C and service temperatures up to 260 °C) [102, 103]. The use of PEEK is increasing in applications ranging from biomedical to high temperature. Filament extrusion and further printing of PEEK is challenging because of the high melting temperature and high expansion upon melting. To achieve high temperatures, several authors

used custom-built FDM systems for processing PEEK [104]. Wu et al. reported that the FDM printed PEEK parts exhibited 108% higher tensile strength, and about 114% and 115% higher compressive and bending strengths, when compared with the FDM printed ABS parts [105]. When compared to PLA, PEEK parts showed 75% improvement in the tensile strength [106].

Thermal management during the printing process, i.e., control of cooling rate highly influences the degree of crystallinity and mechanical properties [107]. A greater amount of fusion is observed in PEEK between different rasters and layers due to high extruding temperatures. Since properties are mainly dependent on the degree of crystallinity, it can be controlled by controlling the nozzle temperature, build chamber and print bed temperatures. Yang et al. investigated the effect of ambient temperature, nozzle temperature on the degree of crystallinity in the printed parts [108]. It is observed that an increase in ambient temperature during printing from 25 °C to 200 °C increases the crystallinity from 17 to 31%, thus improving the tensile strength and modulus of elasticity. Similarly, the degree of crystallinity increases with an increase in nozzle temperature. However, the tensile strength and modulus decreased for nozzle temperatures of more than 420 °C. As shown in Fig. 13, controlling the temperature at the nozzle exit enables printing varying degrees of crystallization in one layer. This gradient in crystallization can be used to tailor the properties of the PEEK printed parts for functional applications.

Kishore et al. reinforced short carbon fibers in PEEK and conducted rheological tests [109]. It is reported that the viscosity of the melt is lower than ABS composites showing the promising nature of processing the PEEK composites into feedstock filaments. Berretta et al. synthesized PEEK and CNT composite specimens with 1 wt% and 5 wt% carbon

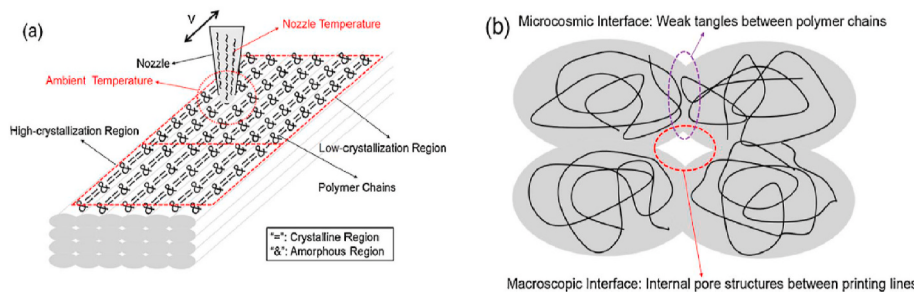


Fig. 13. (a) Varying degrees of crystallinity in different regions of the printed layer (b) microstructure of the printed layers [108]. [Reprinted with permission].

nanotubes (CNT) [110]. The filaments became brittle with the addition of CNT. The presence of pores was observed in the single layer FDM samples of PEEK and its composite. The addition of CNT up to 1 wt%. Increase the ultimate tensile strength. However, the UTS is decreased at 5 wt% of CNTs which may be attributed to pores and agglomerates during printing. Also, tensile samples for short beam shear test were fabricated to find layer to layer bonding. Shear strength of PEEK and 1 wt% CNT PEEK were found to be same, whereas 5 wt% CNT PEEK had a significant decrease. As suggested, surface characteristics (surface tension, wettability and adhesion when molten) are different for 5% than 1% [110]. The thermal and electrical properties of PEEK composites are enhanced by adding both MWCNT and GNP with a reasonable mechanical strength [111]. It is reported that the nano composite with 4 wt % CNT and 3 wt% GNP shows the electrical conductivity of 10 S/m. However, the parts made of FDM using this composition showed a decrease in electrical conductivity due to voids in 3D printed parts.

Combining the advantages of continuous fiber reinforcement in high

strength PEEK and local heating to increase the inter layer adhesion can dramatically increase the properties of the 3D printed parts. To decrease the void formation and increase the inter layer adhesion, techniques such as infrared lamp heating, hot air nozzle preheating and plasma radiation have been used to print low temperature amorphous polymers. However, these techniques will lead to large volume shrinkage. Meng et al. processed continuous carbon fiber reinforced carbon fiber (CF)/PEEK composites [112]. The CF tow is pre-impregnated with PEEK before printing to alter the viscosity during extrusion and to increase the layer adhesion during printing. In addition to pre-impregnation, local heating raises the temperature of the polymer to above glass transition temperature and improves inter layer adhesion (refer Fig. 14).

2.7. FDM of thermoplastic elastomers

Thermoplastic elastomers (TPE) have low modulus, high flexibility and high elongation to breakage. For example, thermoplastic

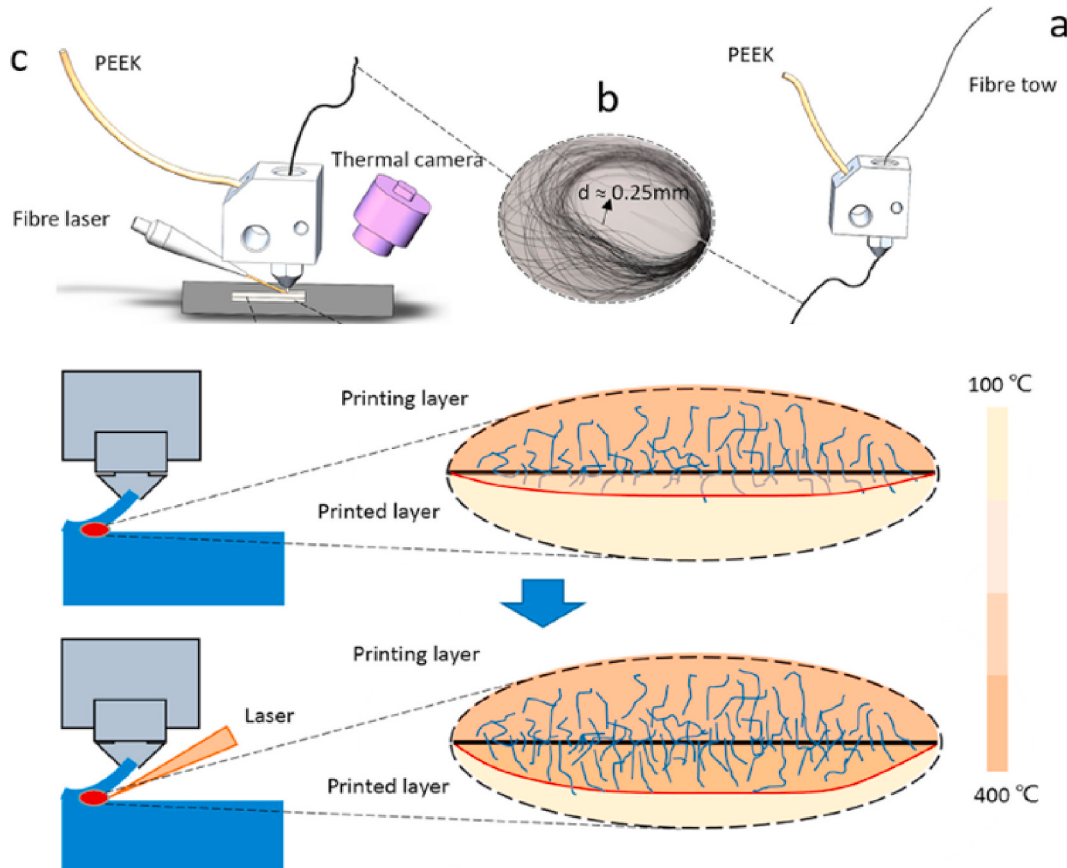


Fig. 14. (a) Pre impregnation of CF tow with PEEK (b) Pre impregnated CF tow (c) FDM printing of the pre impregnated fiber tow with PEEK in presence of local laser heating [112]. [Reprinted with permission].

Polyurethane (TPU) has almost 600% elongation before failure [113]. These are commonly used in applications such as soft robotics, flexible electronic sensors etc. TPE's have low glass transition temperature (T_g) and high crystallization rate and are suitable for FDM processing. However, the FDM of TPE is quite challenging because high viscosity and low elastic modulus make the filament buckling in the nozzle. Kim et al. processed bladders made of TPU by FDM [113]. These bladders are used for manufacturing carbon fiber reinforced composites. To avoid the filament buckling and lateral flow of this soft material during printing, a guide tube with the inner diameter equal to filament diameter is used between the outlet of the filament feeding mechanism and inlet of the hot end. Lin et al. investigated the effect of process parameters during the printing of soft TPU [114]. It is reported that the die swell ratio of the deposited strand increases with temperature. It is reported that the nozzle height influences the interlayer adhesion. As the nozzle height is decreased, fewer voids have been observed in the microstructure, refer Fig. 15.

Christ et al. presented an interesting study on the FDM printing of MWCNT/TPU composite [115]. The addition of MWCNT increased the adhesion. According to the Euler equation, the critical pressure for buckling can be given as

$$P_{cr} = \frac{\pi^2 E d_f^2}{16 L_f^2}$$

where E is the elastic modulus of the filament, d_f is the filament diameter, and L_f is the filament length from the drive gears to the melting zone within the hot end [2]. The critical load is directly proportional to the elastic modulus. The elastic modulus of the TPU composite increases with weight percentage of MWCNT. An increase in elastic modulus greatly assisted in printing without buckling. Therefore, the problem of buckling is mitigated while printing composites based on elastomers. The microstructure of the printed samples shows an excellent interlayer adhesion with no voids, refer Fig. 16. Mechanical and electrical properties are preserved even after FDM 3D printing due to excellent adhesion. This study shows the capability of processing nano composites of soft elastomers and their printing.

2.8. FDM of other thermoplastic materials

The other high performance polymers used in FDM are

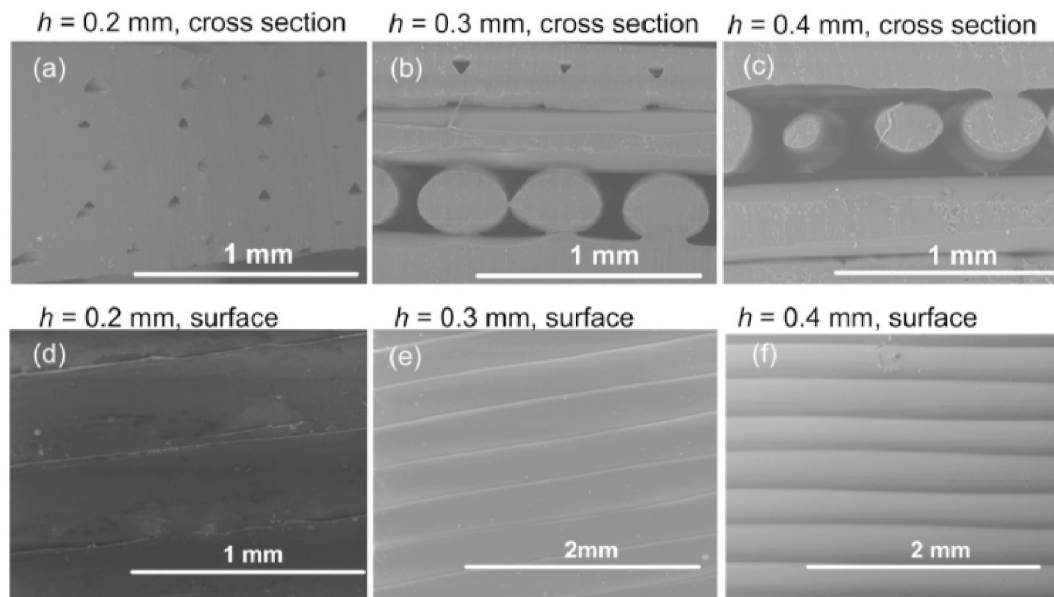


Fig. 15. Effect of nozzle height on the geometry of the cross section [114]. [Reprinted with permission].

Polyetherimide (PEI) and Polyphenylsulfone (PPS). These two polymers are used in various applications due to better mechanical properties and excellent heat resistant properties. PEI is amorphous and has high glass transition temperature (T_g). Jiang et al. suggested that maintaining the nozzle temperature at 370 °C and bed temperature at 220 °C yields better mechanical properties which are close to properties of injection molded parts [116]. Similar to PEI, PPS requires processing temperatures of around 390 °C. The carbon short fiber reinforced PPS composites are suitable candidates for printing tools required for composites manufacturing. For further details, refer [13]. The FDM technology is also used to print other thermoplastic polymers and their composites such as polycarbonate (PC) [117–120], polycaprolactone (PCL) [121]. Similar to other thermoplastics, parts processed by polycarbonate are also highly anisotropic in tensile and shear properties [119]. Shemelya et al. prepared tungsten doped polycarbonate composites. These composite FDM parts showed better radiation shielding properties [120]. The composites made of PCL possess excellent bio compatibility and are mainly used in printing biomaterial scaffolds [121]. Table 1 summarizes the effect of different reinforcements on printing of thermoplastic composites.

3. Applications of FDM

3.1. Biomedical applications

The FDM technology is rapidly used in tissue engineering and in developing patient-specific implants for prosthetics and bones. The complete 3D information and microarchitecture of tissues and organs obtained from Computed Tomography (CT) techniques in the form of image data can be used to process tissues by 3D printing (refer Fig. 17) [122]. The materials that are to be used to process FDM feedstock should possess biocompatibility, along with required mechanical properties [123]. The internal architecture and porosity control of biomaterial scaffolds can be better achieved by 3D printing. By reinforcing bioactive particles into polymers, biocompatible scaffolds can be processed using FDM technology [124,125].

In tissue engineering, processing of scaffolds with controlled porosity and interconnected network is challenging as the traditional scaffold processing techniques lack in incorporating the desired network. The use of FDM technology has been increasing in printing the biocompatible composite scaffolds with better control of pore size and distribution.

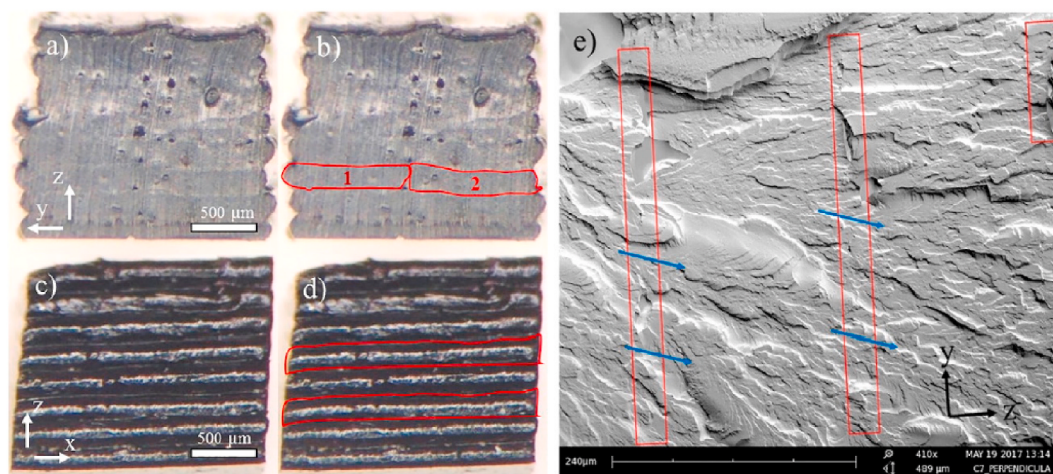


Fig. 16. Structure of TPU/3 wt%MWCNT: a) cross-section, and b) cross-section with highlighted extrudate layers in y-direction, d) profile with two highlighted extrudate layers e) SEM micrograph showing y-z view of the interlayer bonds. The red rectangles show the interlayer areas and the blue arrows indicate the regions where the failure flows across the interlayer regions [115]. [Reprinted with permission]. (For interpretation of the references to colour in this figure legend, the reader is referred to the Web version of this article.)

Zein et al. processed biomaterial scaffolds by using a bioresorbable polymer polycaprolactone (PCL) as filament material [126]. Different interconnected network structures with 0/90° and 0/60/120° layer orientation with rectangular and honeycomb pores patterns are printed. Analysis of mechanical properties of these PCL scaffolds through compression tests revealed a high correlation between the scaffold porosity and compressive properties. To improve the hydrophilicity, adhesion and mechanical properties, biocompatible materials such as tricalcium phosphates (TCP) and hydroxyapatite (HA) are added. Davilia et al. fabricated PCL + TCP composites and fabricated scaffolds by 3D mini-screw extrusion printing (refer Fig. 18) [122]. It is reported that 20 wt% of TCP shows an excellent mechanical properties and about 107% increase in compressive modulus of scaffold is observed. Scaffolds of different complex architecture have been printed by using a particulate composite consists of polypropylene (polymer) and tricalcium phosphate (ceramic) [127]. The composite architecture with a porosity of 38 vol % showed better compressive strength.

Few studies also reported *in vivo* experiments of these printed scaffolds. The biocompatible PLGA/TCP/HA composite scaffolds have been processed through FDM technology and implanted into rabbit femoral bone defect to support bone deposition and scaffolds are biodegraded over time [128]. Kabirian et al. investigated the printing of synthetic vascular scaffolds [129]. The authors 3D printed PLA scaffold using FDM and did *in vivo* degradation studies and found that PLA scaffold degradation is slow enough to provide the required mechanical support during cell growth, which opens up the possibility of using this technique for tissue-engineered vascular grafts. Woodfield et al. characterized the three dimensional poly (ethylene glycol)-terephthalate-poly (butylene terephthalate) (PEGT/PBT) block copolymer scaffolds for engineering of articular cartilage [130]. In addition to these, nanoparticles such as MWCNT, graphene, Fe₃O₄ are added to increase the functionality of these scaffolds. The composite consisting of magnetic Fe₃O₄ particles, mesoporous bioactive glass (MBG) and PCL is extruded in a paste form to print multifunctional scaffolds that show better osteogenic activity [131]. 3D printable composite inks containing graphene and biopolymers can be used for printing multifunctional biocompatible devices. In this process, the composite liquid ink rapidly solidifies upon extrusion and is deposited layer wise on the build platform [132].

Other critical applications of FDM is in the processing of orthopedic implants and dental applications. Currently, most of the implants are processed using metal alloys such as titanium (Ti), but these metallic biomaterials have certain limitations. Bio compatible polymers such as PEEK and its composites shows modulus close to the human bone (14

GPa) and can be processed in a filament form to further use in 3D printing. Han et al. reported that the addition of 5 wt% carbon fibers increase the mechanical properties and when 3D printed, the properties are close to injection molded pure PEEK samples [133]. PEEK-CF composite is bio compatible and has high mechanical properties than pure PEEK when 3D printed. Antoniac et al. printed anterior cruciate ligament (ACL) using the composite made of PLA, magnesium and Vitamin-E. The processed composite contains good biocompatibility and osteo conductivity [73]. The bio-model of the patient jaw has been prepared using FDM in Ref. [124]. A customized, patient specific jaw has been processed. Three dimensional slice sections of the jaw obtained from CT and MRI are translated into stl file and used for printing. The main advantage of using FDM is the user's ability to make a highly customized product on site with very little lead time. This makes the technology to use for quick processing of wound healing materials [74] and pharmaceutical drugs [134,135]. The advantage here is "Individually tailored oral drug dosage" or "One's own medicine" [134,135]. The main advantage of FDM and 3-D printing in the biomedical field is the high degree of customization (dosage, size and shape) and the ease of manufacturing in case of implants (Orthopedic and otherwise), wound/burn dressing materials, oral delivery systems (Tablets) etc.

3.2. Electronic and functional applications

The development of polymer composites with tailored electrical properties and good feedstock filament processability allowed researchers to use FDM for printing parts for dielectric, conductive, sensor and energy storage applications. For instance, high relative permittivities of ceramics and the processability of thermoplastics can be combined to print dielectrics. Castles et al. demonstrated that the 3D printed ABS-BaTiO₃ composite part have dielectric properties in a similar range to bulk specimens provided the quality of the printed part is very high without any voids [136]. With optimum control of the print parameters, there is a scope to use FDM for printing materials for dielectric applications such as passive antennas. Carbon based fillers provide conductive paths inside polymers and can be used as a replacement for copper filler, which has an oxidizing tendency. The carbon based polymer composites can also be readily processed into filament form with relatively less cost. Nowadays, different composite feedstock filaments with conductive fillers are commercially available. For instance, conductive PLA/graphene filament from BlackMagic®, PLA/carbon black filament from Proto-pasta® and Electrify from Multi3D®. These filaments have a volume resistivity in the range of 0.6 Ω-cm to 30 Ω-cm [137–139].

Table 1

Summary of the effect of reinforcement on FDM printing of composites.

Composite	Property improvement	Remarks	Ref.
ABS + Vapourgrown carbonfibre (VGCFs)	Tensile modulus increased by 44% at 5 wt % filling. No surface interaction with the polymer.	Preferred orientation due to extrusion showed improved mechanical properties. But, properties of printed parts are less due to voids.	[45,46]
ABS + SWNT	Tensile modulus increased by 93% at 5 wt% filling.	Some surface interaction, even without functionalization. Better properties than VGCFs.	[45,46]
ABS + TiO ₂	Ultimate tensile strength (UTS) increased by 13% in XYZ and 30% in ZXY. Tensile modulus increased by 11% in XYZ and 14% in ZXY at 5 wt% filling.	Dispersion issues can be solved using silanes. Lower surface roughness in printed parts. Void percentage is reduced in printed parts.	[58]
ABS + BaTiO ₃	Relative permeability increased by 260% at 35 vol%. Flexural strength decreased with increase in filler volume, 53% decrease was reported at 30 vol% loading.	Increasing filler load makes the filament more brittle. Printing can be done reliable upto 35 vol% loading. Above 45% loading, stick-slip behavior was observed	[62]
ABS + Shortcarbon Fibers	Tensile strength increased by 70% and flexural strength increased by 18.7%.	Poor interface, fiber pullout has been observed. Void content increased in printed parts.	[47]
ABS + BN flakes	Negative impact on flexural properties. Increase in filler material leads to an increase in thermal conductivity.	Agglomeration and void content is higher in printed parts.	[60]
ABS + OMMT	Tensile modulus increased by 200%, strength increased by 44%, linear expansion coefficient decrease by 36% at 5 wt% loading.	Glass transition temperature (T_g) and thermal stability is increased. Improvement in mechanical properties of printed parts.	[50]
ABS + Jutefibres	UTS decreased by 9% in XYZ and 8.5% in ZXY. Tensile modulus increased by 1% in XYZ and decreased by 26% in ZXY at 5 wt % filling.	Decomposition of jute fibres during extrusion and printing leading to additional porosity in printed parts.	[58]
ABS + Cu	UTS decreased by 42% and tensile modulus increased by 4% at 30 wt% loading. Coefficient of thermal expansion decreased by 30% and thermal conductivity increased by 41% at 50 wt % loading.	Distortion of printed parts decreased with Cu addition	[61]
ABS + Shortcarbon fibers	The tensile strength is increased with carbon fibers. The composite became brittle.	Poor adhesion for longer fiber lengths.	[65]
PLA + Graphene	A 14% enhancement in wear resistance was observed. T_g decreased by 16%.	Due to decrease in T_g , weak interlayer bonding was observed in composite printed parts.	[67]

Table 1 (continued)

Composite	Property improvement	Remarks	Ref.
PLA + Graphene	Increase in tensile strength, decrease in flexure strength.	Printed parts showed a huge anisotropy. Printing in upright position decreases properties by 30%	[68]
PLA + CNT	Filament fracture strength increased by 275%.	CNT has a higher heating ability than graphene when exposed to microwave. High inter layer adhesion is observed with microwave heating.	[69]
PLA + CNT + GRAPHENE Bi-filler	Enhanced electrical conductivity.	Bi-filling is an easy way to minimus agglomeration. Printed parts showed beter properties.	[70]
PLA + Lignin (LIG)	Decrease in fracture resistance of filament beyond 0.5 wt% loading.	Printed composite parts showed antioxidant properties.	[71]
PLA + Mg with vitamin E	A decrease in T_g was observed due to the addition of Mg. No effect on adhesion and surface morphology of the deposited filaments.	Vitamin E helps in better integration of Mg into the PLA matrix and reduced probability of Mg oxidation.	[73]
PLA + Continuous carbon fiber	Improved adhesion and mechanical properties by using methylene dichloride as sizing agent.	Tensile strength of printed parts increased by 14% and flexure strength by 168%. This example demonstrates the importance of coupling agents for improving fiber/matrix adhesion.	[74]
Nylon + Fe	Small size fillers increases tensile elongation and large size fillers increase tensile modulus.	Die length should be increased during printing.	[77]
Nylon + Al ₂ O ₃	90% cheaper filament than ABS-P430 filament with similar MFI. Lower Mechanical properties.	The nylon used was recycled. Reduction in melting temperature and crystallinity. Particle size more than 150 μm caused nozzle clogging.	[79]
Nylon + Zirconia (15%) and β -TCP	Tensile strength decreased by 34%, tensile modulus increased by 10% at 40 wt% loading	Due to agglomeration, nozzle clogging was reported for particles sizes of 400 μm .	[82]
Nylon + Graphene nanoplates	Increase in tensile modulus by 50%, 48% and 40% for specimens printed at 0°, 45° and 90° orientation, respectively. Decrease in UTS by 7%, 5% and 8% for 3D printed 0°, 45° and 90°, specimens, respectively.	Extrusion induced orientation phenomenon of GNP observed. Extrusion speed increased the degree of orientation.	[83]
Nylon + Glass continuous fiber	The isotropic pattern yields excellent properties in tension and	The tensile strength at 33 vol% of glass fibers printed in a concentric pattern matches the	[85]

(continued on next page)

Table 1 (continued)

Composite	Property improvement	Remarks	Ref.
	concentric pattern yields better properties on bending.	strength of aerospace grade aluminium.	
Nylon + Kevlar continuous fibre	An increase in tensile modulus. Concentric rings of fibers are embedded around the product geometry. Sample failure occurs at the start of the kevlar fibres.	Mechanical properties of printed parts increased with increase in number of concentric rings i.e. volume fraction of continuous fiber reinforcement.	[86]
PP + Glass fibres	Composite reported a lower MFI. Printing was done at a higher temperature (185°C).	The reinforcement successfully countered loss in mechanical property due to printing, i.e. printed composite UTS is nearly equal to the UTS of compression molded PP.	[88]
PP + expanded-perlite	Small sized fillers enhance the filler-matrix adhesion, reduce the polymer chain orientation and constrain the polymer from shrinking.	Increase in the build chamber temperature alters the morphology of the crystal growth and decreases warpage.	[89–91]
PP + Glass	Tensile modulus increased by 280% and UTS increased by 62% at 30 wt% loading	The distortion of printed parts is high.	[92]
PP + Hemp	Tensile modulus increased by 201% and UTS increased by 71% at 30 wt% loading. Net reduction of 78% was observed in shrinkage.	Sharskin effect was observed on the filament surface.	[92]
PP + Harakeke	Tensile modulus increased by 210% and UTS increased by 74% at 30 wt% loading. Net reduction of 84% was observed in shrinkage.	Better performance than Hemp. However addition of natural reinforcements decreased the distortion of the printed part.	[92]
PP + Gypsum	Net reduction of 46% was observed in shrinkage values at 50 wt% loading	Increase in gypsum loading leads to agglomeration and nozzle clogging.	[92]
PP + Carbon black	Resistivity below $10^{-2}\Omega\text{m}$ was achieved with 30 wt %	Better thermal stability than PLA-Graphene based Composites.	[141]
PE + Al_2O_3	The MFI of composite is less.	Printed parts showed better wear resistance and thermally stable.	[95]
PE + glass powder	Improvement in the wear resistance by 50%.	Printed parts showed better wear properties for low load applications.	[96]
PE + TMP	Adhesion is increased by adding maleic anhydride compatibilizer	Printed parts showed better biocompatibility with high mechanical properties.	[97]
PETG + CNT			[100]

Table 1 (continued)

Composite	Property improvement	Remarks	Ref.
		Improve in mechanical properties	The void content is lesser in the printed parts.
PEEK + Carbon fibre	Five wt.% milled carbon fibres with a length of 80–150 μm and a diameter of 7 μm was used as the filler. Tensile strength increased by 94% and UTS increased by 7%. No statically significant change in compressive properties.	Printed parts has required roughness to use in dental applications.	[133]
PEEK + CNT	The addition of CNT increases the tensile strength, but filaments became brittle.	The presence of pores was observed in printed parts.	[110]
PEEK + Bi-filler (MWCNT + GnP)	Tensile modulus of the filament increased by 28% at 4 wt% CNT and 3 wt% GNP loading. Increase in electrical and thermal conductivity is also observed for bi filler addition.	Re-agglomeration during reheating. Electrical conductivity decreased after printing	[111]
TPU + MWCNT	At 5 wt% of MWCNT, the elastic modulus of the printed part is almost equal to the bulk specimen (only ~14% less)	Excellent layer adhesion has been achieved with increasing in MWCNT during printing	[115]

These conductive filaments can be used in FDM to print either the embedded devices or the entire electronic circuits. Flowers et al. demonstrated the capability of printing capacitors, resistors and inductors using these conductive filaments [140]. The same study also demonstrated the printing of embedded hardware like LED. As shown in Fig. 19, a cavity has been created in a CAD model similar to the dimensions of the LED. The printing process is stopped at the top of the cavity, LED was manually placed and then the print is resumed by printing the conductive traces over the top of the LED. This is later connected to the battery to light LED. This example shows the capability of printing a variety of components used for electrical applications.

Leigh et al. demonstrated the printing of piezoresistive and capacitive sensors using the carbon black filled polycaprolactone (PCL) composite filaments [22]. The printed piezoresistive sensors were able to sense the mechanical flexing when the electrical resistance is changed. The custom capacitive sensors embedded in smart vessels can detect the presence of water (refer Fig. 20). Kowk et al. developed low cost and highly thermally stable PP/carbon black composite feedstock filaments [141]. The printing of temperature sensors and flex sensors has been demonstrated. Prashantha et al. obtained 10 wt% commercially available PLA-graphene filament, which has higher dielectric properties than PLA. These composite filaments can be used to make EMI shield [142]. Zhang et al. reported that reducing graphite in a two-step reduction process (chemical exfoliation and thermal reduction) yields the resistivity of 0.0016 Ωcm for the rGO [143]. The authors processed rGO-PLA composites through melt blending and reported a volume resistivity of 0.21 $\Omega\text{ cm}$ for the composite (at 6 wt% loading). This is better than the commercially available graphene/PLA filaments. Using these

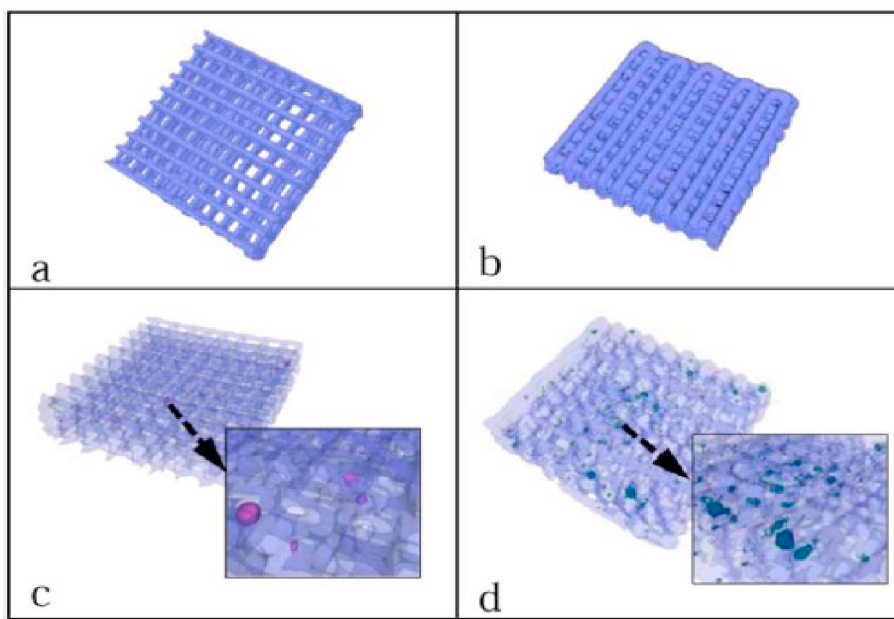


Fig. 17. The 3D reconstructions generated from μ -CT data for scaffolds [122]. [Reprinted with permission].

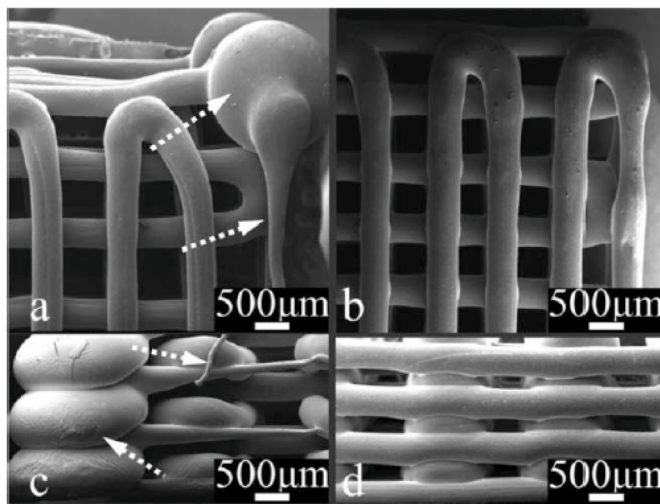


Fig. 18. SEM micrographs of PCL scaffolds: (a,c) morphological defects (arrows point to the defect location) and (b,d) morphology without defects [122]. [Reprinted with permission].

rGO/PLA composites, the authors demonstrated the printing of flexible 2D and 3D circuits.

The other promising application of FDM is printing devices used for electrochemical energy storage. Several studies have reported the use of ink deposition techniques for printing electro chemical energy storage devices. These techniques require separate steps for the in-situ curing and polymerization after. FDM provides the capability to directly print these devices without further curing steps. Rymansaib et al. demonstrated FDM printing of electrochemical sensor using polystyrene-MWCNT-Graphene composite [144]. Foster et al. made an 8% graphene and 92% PLA Filament and used FDM to make an electrode in a disc shape and used it in a Li-ion battery as an anode and a solid-state super capacitor [145]. Even though it is not very good compared to other products available in the market, as a proof of concept, there is a lot of scope for future research. The main challenge here is the ability to form a good quality dispersion [145,146]. Kim et al. demonstrated the printing of multi-axial force sensor by simultaneous printing of the

structural and sensing parts [147]. As shown in Fig. 21, the supporting structure is printed with flexible TPU and sensors are printed using functional CNT + TPU nano composite. This simultaneous multi nozzle 3D printing allows the preparation of multi axial sensors in one step. Previously, these sensors are fabricated by assembling individual sensors. The piezoresistive property of the composite can be utilized to fabricate haptic devices.

3.3. Tooling applications

The research group at ORNL has done an extensive work on printing molds and tooling required for composite fabrication. For further details, refer [148–153]. Molds required for hand layup, vacuum assisted resin transfer molding (VARTM), compression molding, etc. are printed using the BAAM facility. Techniques such as machining an oversized mold or coating an undersized mold are used to maintain the surface quality of molds. The total manufacturing time and cost involved with printing are less compared to the conventional mold manufacturing techniques. Hassen et al. 3D printed mold using the ABS composite reinforced with 20 wt.% short carbon fibers [148]. This mold has been used to prepare carbon fiber reinforced composites using VARTM. These molds are durable that after fabricating and removing composites, they retained dimensional stability. Sudbury et al. printed tools used for hand layup technique [149]. Both planar and curved molds have been printed, as shown in Fig. 22. The planar mold is coated with epoxy grades and curved molds are machined to maintain the surface quality. A 6-ply fiber glass composite has been fabricated using this printed hand lay up tools. The durability of the tool is assessed by the number of pulls of the fabricated composite. It is reported that the durability of printed parts and total cost involved in printing is less than the conventional techniques. For further details, refer [9].

Complex hollow composite parts can be prepared by Bladder Assisted Composite Manufacturing (BACM). As shown in Fig. 23, manufacturing of outer molds and bladder using traditional techniques involves complex processes. The aluminum molds provide the outer surface finish and bladder provides the inner surface finish for the hollow composite. Kim et al. demonstrated the printing of the bladder using TPU [113]. Since TPU is soft, different trials have been conducted to find the optimum print and process parameters. This bladder was used in consolidating and curing of the carbon fiber reinforced composite

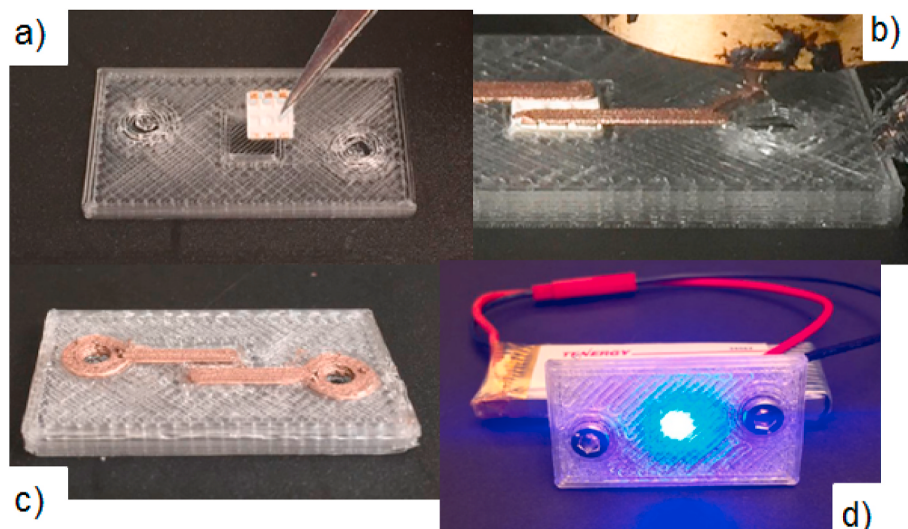


Fig. 19. a) printing process is paused and LED is placed into the cavity before resuming the print. B) printed conductive traces on top of LED contacts c) Fully embedded LED component d) screw terminals are used to attach a battery and to light the LED [140]. [Reprinted with permission].

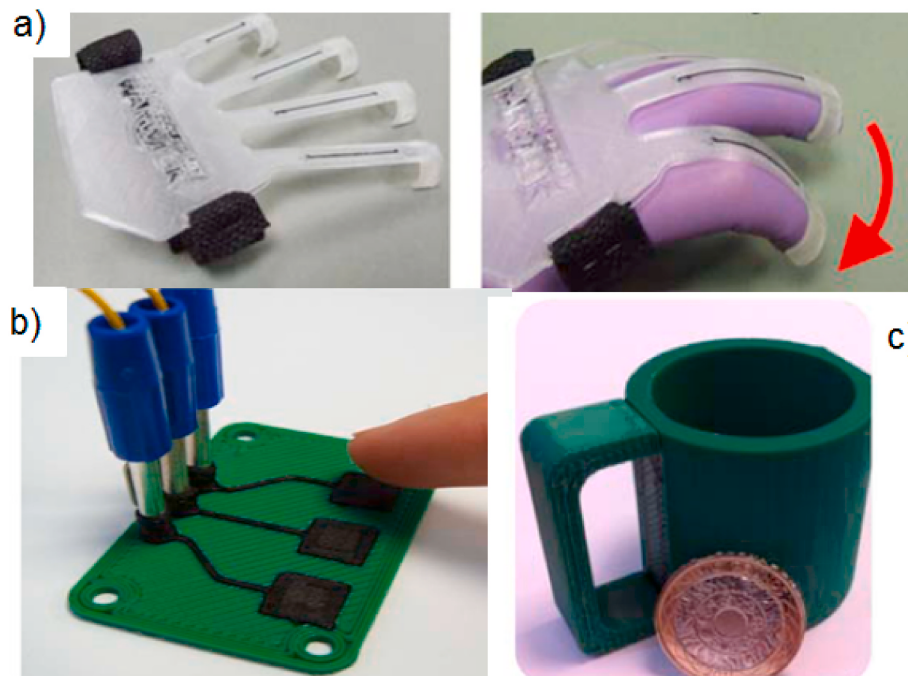


Fig. 20. FDM printed a) piezo resistive sensors b) Capacitive sensors c) smart vessels [22].

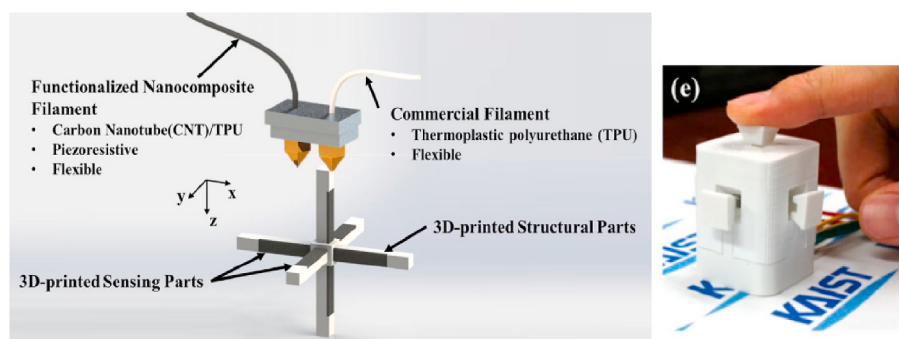


Fig. 21. Schematic design of the 3D printed multi axial force sensor and haptic device [147]. [Reprinted with permission].

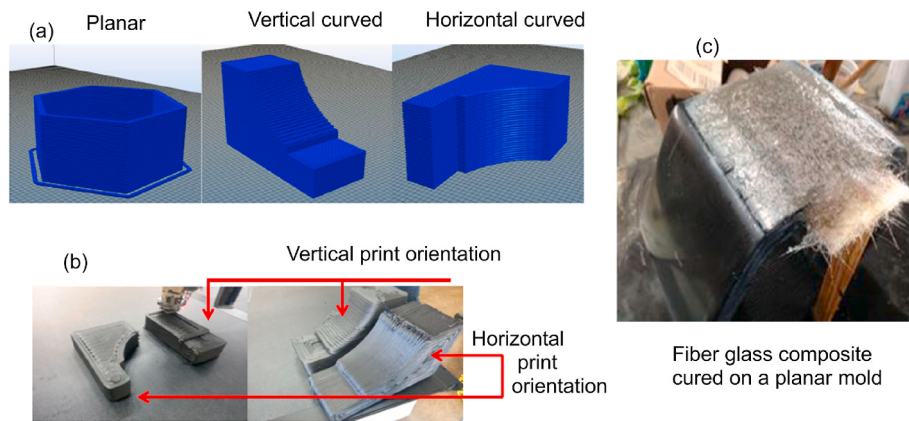


Fig. 22. a) CAD diagrams of the planar and curved molds b) during and after printing of the curved parts and c) fiber glass composite cured on a planar mold [149]. [Reprinted with permission].

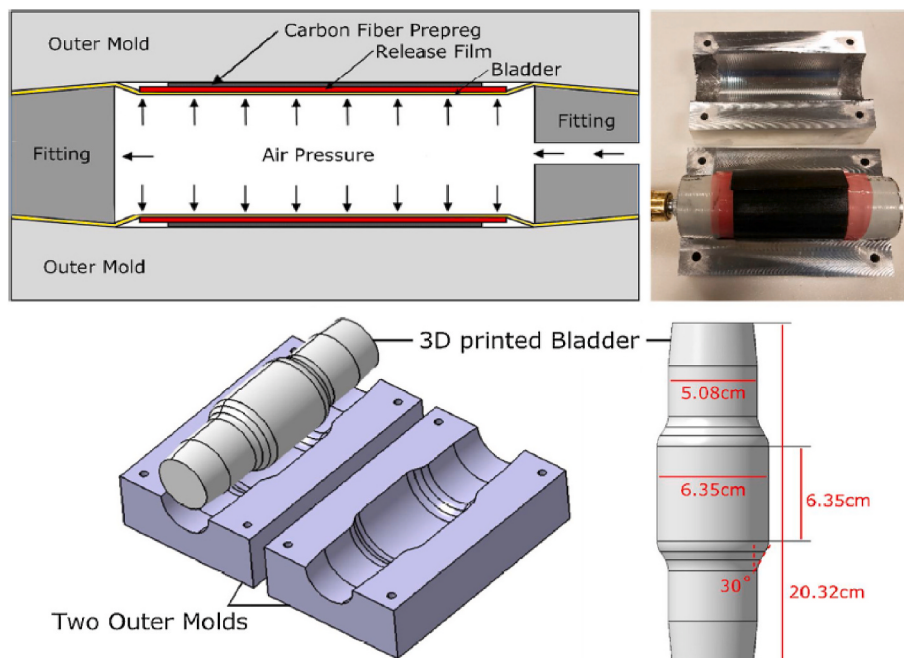


Fig. 23. FDM printed bladder used in bladder assisted composite manufacturing [113]. [Reprinted with permission].

cylinders. It is reported that the void content in the fabricated composite parts is less than 1%, which is less than traditional techniques. These composites with less void content are suitable for aerospace applications.

3.4. Aerospace applications

FDM is a quicker and cost effective process for processing complex geometric parts required for unmanned aerial vehicles (UAVs) [154]. In collaboration with Aurora Flight Sciences, Stratasys® printed a jet engine UAV which weighs only 33 pounds [155]. Almost 80% parts of this light weight UAV are processed by additive manufacturing. Majority parts are printed using FDM. For example, honeycomb structures inside wings etc. Materials such as Ultem® (a trademark resin of PEI) and Acrylonitrile Styrene Acrylate (ASA) were used. Further developments on the use of FDM in printing UAVs were given in Ref. [154,155]. The parts used in aerospace applications generally should contain very minimal void content. The mechanical properties of printed parts must match with the requirement of aerospace components. As the FDM

printed parts have void content and anisotropic nature, processing parts required for aerospace applications by FDM is quite challenging. If the 3D printing technology is successfully explored, there is a scope of saving manufacturing time and fuel [156]. Use of reinforced composites also increasing to increase strength of UAV parts. Gardner et al. processed PEI/CNT composite filaments with enhanced mechanical and electrical properties [157]. The UAV frame has been successfully printed using this composite. As shown in Fig. 24a, free ends of printed quadcopter made of CNT yarns can be attached to rotors. Fig. 24b shows the assembled quadcopter with rotors in motion. Azarov et al. printed a composite frame structure for unmanned aerial vehicle (UAV) [158]. In this work, carbon fiber tows are reinforced with thermoplastic material during printing. The process and the frame structure are shown in Fig. 25. Both theoretical and experimental analyses have been performed on the printed structure to check its performance. It is reported that the structure has high stiffness and low deflection. It can resist the payload up to 294 N without much changes in the geometrical dimensions.

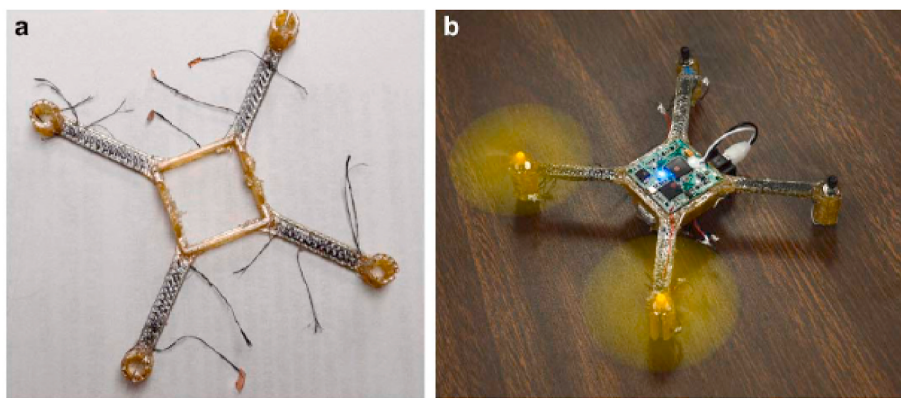


Fig. 24. a) PEI nanotube in PEI frame b) Quadcopter with motor powered via CNT yarn [157]. [Reprinted with permission].

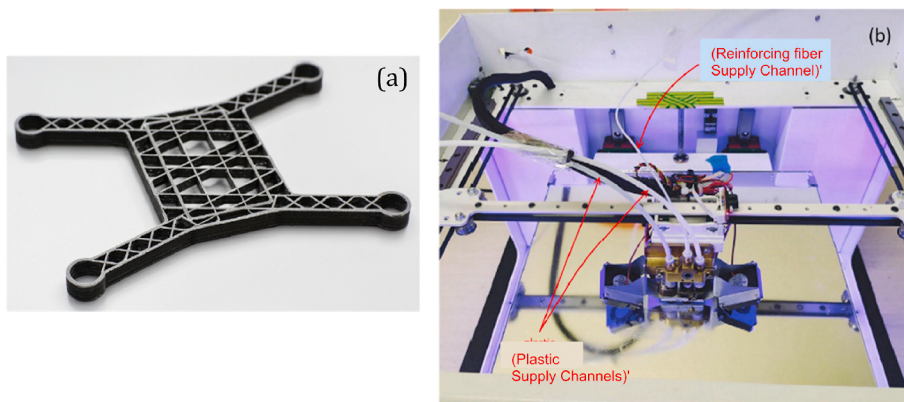


Fig. 25. 3D printed UAV composite frame [158]. [Reprinted with permission].

4. Mathematical modeling

Mathematical models provide useful information to understand the effect of different physical phenomena on the properties of printed parts [159]. Several key inputs can be obtained through these models to optimize the printing process to get quality products [160]. These mathematical models are categorized in this work as the models for simulating the printing process itself and models for estimating the mechanical behavior of printed parts. Numerical techniques such as Finite Difference (FD) and Finite Element (FE) methods have been used in the literature to simulate the flow field and reinforcement orientation in the extruding nozzle, temperature and thermal stress fields during the solidification and the distortion of the printed parts [161]. The mechanical properties of the printed parts can be analyzed using analytical techniques such as classical laminate plate theory (CLPT) [162] or using homogenization techniques [163].

4.1. Printing process modeling

The melt flow behavior is crucial during the printing of particulate and short fiber reinforced composites in determining the processability. The random orientation of fillers in the thermoplastic material changes the viscosity of the melt and affects the flow of material through the die. Further, the anisotropic behavior of printed parts is sensitive to the deposition of reinforcement on the printed layers. Process parameters such as printing speed, filling rate, melt viscosity and volume fraction etc. Determines the distribution of filler materials. Few literature works analyzed the melt flow behavior and the flow induced fiber orientation during the extrusion of short fiber reinforced composites [164]. The accuracy of these studies depends on the models used for describing the

melt flow and fiber orientation. Nikzad et al. investigated the flow behavior of iron particle reinforced ABS through the liquefier head using the 2D and 3D models built in ANSYS^C [165]. The temperature, pressure drop and velocity profiles have been simulated by representing the rheological behavior of the melt with a power law. Gracia et al. investigated the fiber alignment at the exit of a diverging nozzle [166]. The authors used Mold flow software with Folgar-Tucker model to describe fiber orientation and assumed that the flow exits the nozzle to a large open cavity, which is an output boundary condition. It is observed that the fibers are highly oriented along the flow direction. Heller et al. considered the die swell effects at the nozzle exit and reported that the die swell reduces the fiber alignment at the nozzle exit and also reduces the axial modulus by 20% [167]. In this work, the melt is considered to be Newtonian fluid. Lewicki et al. modeled the flow of short carbon fiber through the nozzle [168]. In this study, short fibers have been considered as the discrete particles. Fluid dynamics approaches have been used to model the particle-particle, particle-melt and particle-wall interactions. Initially, random fiber orientation is assumed. As shown in Fig. 26, fibers are aligned along the flow direction in the nozzle during the extrusion process. The high amount of orientation is observed on the walls. It is to be noted that both the continuum based and discrete modeling approaches of fluid flow are computationally expensive.

The properties of the printed parts depend on the bond formation between the beads. Many mathematical models are presented to analyze the sintering, dynamics of neck formation and growth during the bond formation in FDM of thermoplastic materials [9,15,17]. These models to predict the bond strength are validated with the experiments that determine the fracture strength of printed parts [169,170]. However, further mathematical works are required to incorporate the effects of reinforcement size and shape on the neck formation and growth.

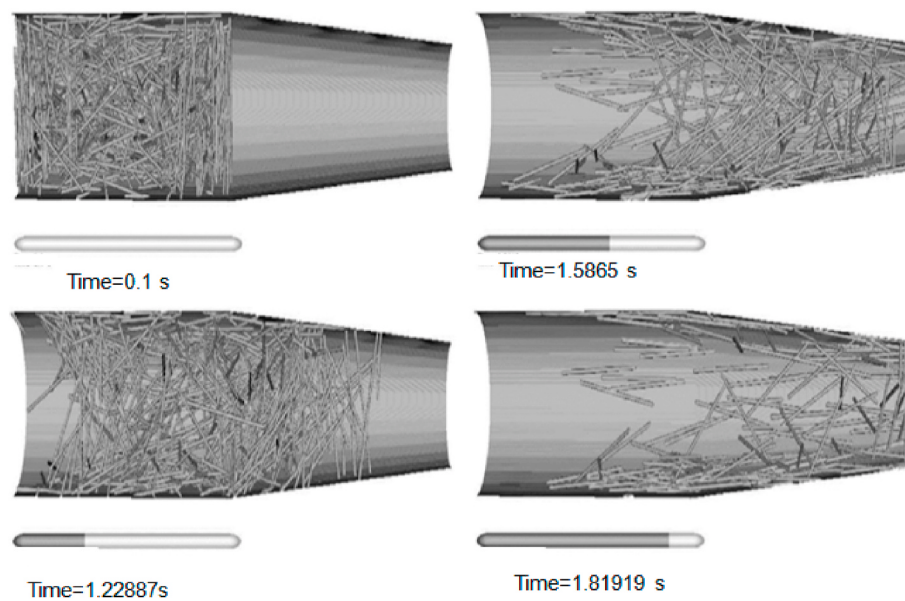


Fig. 26. The flow of fibers through the nozzle. The reinforced fibers are considered as discrete particles for modeling purpose [168].

The study of the solidification behavior, the evolution of temperature and thermal stress profiles and the associated deformation is crucial because the residual thermal stress field determine the part warpage and strength. Many analytical and numerical models have been presented for simulating the FDM printing of unreinforced polymers. Earlier works predicted the relations for the bond potential based on 1D heat transfer models [171]. The deposited beads are considered as 1D rigid blocks and interactions with other beads are modeled by assuming heat sink terms. Belleheumer et al. developed a lumped heat capacity model by assuming the elliptical cross section of beads and constant surface temperature [15]. Thomas and Rodriguez proposed steady state 2D analytical heat transfer models by assuming the cross section of beads as rectangular and imposing free convection boundary conditions [172]. Numerical models generally simulate the layer wise manufacturing processes using layer wise activation of the computational domain [173,174]. For example, as shown in Figs. 27 and 2D computational domain of thickness equal to the print layer thickness is considered. The convection heat transfer to the bed and ambient is considered as boundary conditions on the respective boundaries. As the time progress, a new layer of the computational domain is added in the vertical direction to represent the growth of the printed parts. A constant surface temperature boundary condition is given to the top boundary to represent the freshly deposited layer. Realistic 3D transient numerical models are presented using the FE based commercial software by incorporating the realistic convection boundary conditions and by considering the temperature dependent material properties. Zhou et al. simulated the FDM process in ANSYS® by stepwise activation of beads [175]. The temperature dependent

conductivity and heat capacity are considered. Costa et al. presented an accurate analysis by considering the convection and radiation within the print environment and thermal resistances between the beads [176]. It is reported that the convection conditions significantly influence the temperature profiles.

The crystallization phenomena affects the heat transfer to a great extent. Brenken et al. presented a 2D transient heat transfer model strongly coupled with a crystallization kinetics [177]. The authors used the crystallization model developed by Velusaris and Seferis [178] to model the crystallization kinetics of PEEK, which can also be used to model crystallization kinetics of fiber reinforced polymers [179]. In this study, the printing process is replicated with a stepwise activation of beads and thermal and crystallization profiles are predicted for different packed bed geometries. The heat released during crystallization is coupled with heat transfer through the source term. Further details about the model and boundary conditions are given in Ref. [180,181]. This model provides an important aspect of the crystallization behavior of the reinforced semi crystalline polymers and the temperature results of this model can be used as an input to further residual stress analysis. The authors further extended the model for a complete 3D analysis built using ABAQUS®. The printing process is replicated with the step wise activation of the elements and the solidification behavior of the deposited beads are molded by considering convective and radiative heat transfer. When the heated layer comes in contact with the already solidified layer, there may be a chance of re-melting. The authors implemented both crystallization and re-melting effects using the user ABAQUS® subroutines.

The non-uniform thermal gradients and the viscoelastic material behavior of the polymer needs to be considered to predict thermal stress and distortion. Wang et al. proposed an analytical solution to quantify the intra-layer deflection and inter-layer deformation (warp deformation) based on elastic solutions [182]. The stresses induced during the cooling from the glass transition temperature to build chamber temperature are only considered in this work. Xinhua et al. presented a thermoelastic analytical solution for analyzing the distortion of FEM printed PLA thin plates [183]. This analytical solution has lot of limitations. Zhang et al. presented a full 3D analysis in ANSYS® to investigate the effect of process parameters such as printing speed, bead width and layer thickness on the residual stress and final distortion of the printed part [184]. A coupled thermal analysis is performed using the thermoelastic model and step wise activation of the printing process.

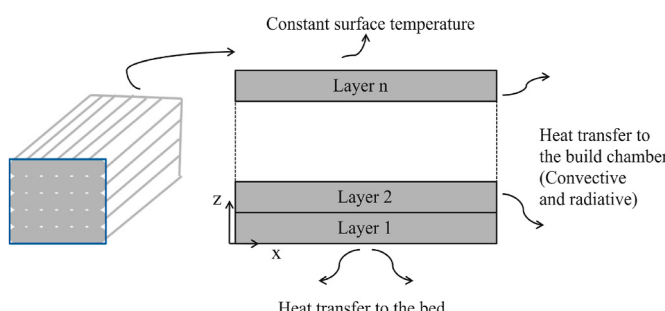


Fig. 27. Simulation of the FDM process using layer wise addition of computational domain.

The printing speed has a high influence on the part distortions. Recently, few works are published to study the thermomechanical behavior of fiber reinforced polymer printed parts. Talagani et al. presented the fully coupled thermomechanical FE model of a car chassis printed using Extrusion Deposition additive manufacturing using carbon fiber reinforced ABS [185]. The machine code has been used for printing. The thermal and mechanical material properties required for the study have been calculated using homogenization approaches. In the FE simulation, local material orientations are assigned using the bead local directions.

4.2. Models for the analysis of mechanical behavior

Many analytical and numerical techniques are presented in the literature for analyzing the mechanical behavior of FDM printed thermoplastic parts [186]. Crocolo et al. proposed an analytical solution by considering the inclined filaments as inclined truss members and the adhesion between rasters has been determined empirically [187]. Huang and Singameni reported an analytical solution to study the effect of raster orientation by considering the filament cross section as a square with elliptical curvature at the edges [188]. The mechanical properties are sensitive to both the degree of coalescence and the raster orientation.

Existing micro and macro mechanics models for laminated composites can be applied to 3D printed composite parts due to the layer wise printing nature of the process. As shown in Fig. 28, micro mechanical models consider the interaction between the beads and interface effects between fiber and polymer. Each layer of the FDM printed part can be considered as an orthotropic lamina. The longitudinal stiffness of this lamina can be found from the modified rule of mixtures as,

$$E_L = \chi_1 \chi_2 V_f E_f + V_m E_m \quad (1)$$

where χ_1 and χ_2 are the factors introduced to take into the effect of reinforcement orientation, aspect ratio etc. For continuous fiber reinforcement, these factors may be equal to 1 [189]. The variables V_f and V_m represents the volume fraction and E_f and E_m represents the modulus of fiber and matrix, respectively. The transverse stiffness and shear modulus of the lamina are generally estimated using Halpin-Tsai model, which is written as

$$\frac{E_T}{E_m} = \frac{1 + \xi \eta V_f}{1 - \eta V_f} \quad (2)$$

$$\frac{G_{LT}}{E_m} = \frac{1 + \xi \eta V_f}{1 - \eta V_f} \quad (3)$$

where, the parameter ξ and η are shape factors representing the size and shape of reinforcements [190]. For nano particle fillers of spheroidal shape, Mori-Tanaka average stiffness model is used to estimate the longitudinal and transverse stiffness values as,

$$\frac{E_{11}}{E_m} = \frac{A}{A + V_f(A_1 + 2V_m A_2)} \quad (4)$$

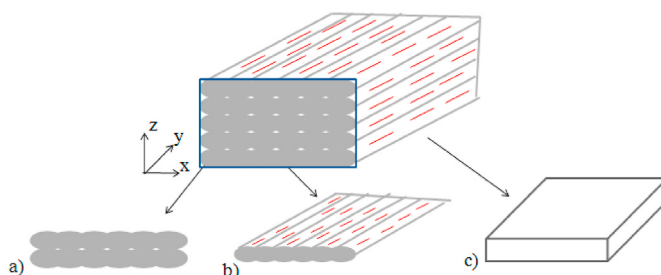


Fig. 28. Various levels for analysis a) micromechanics b) single lamina and c) laminate.

$$\frac{E_{22}}{E_m} = \frac{2A}{2A + V_f(-2V_m A_3 + A_4(1 - V_m) + A A_5(1 + V_m))} \quad (5)$$

where V_m is the Poisson's ratio of the matrix and $A, A_1, A_2, A_3, A_4, A_5$ are functions of Eshelby's tensor [191,192]. These analytical models are valid for layers printed with zero airgap. However, the final microstructure of the FDM printed layer parts contains voids. The theoretical predicted modulus values can be modified to account for the effects of voids as [193],

$$E_c = \zeta(1 - \rho_{void})E_t \quad (6)$$

where E_t is the theoretical elastic property without voids, ρ_{void} is the void density and ζ is the empirical factor representing the bond strength. The void density can be calculated approximately from the meso structure. Thus, the stiffness matrix of each layer can be written as

$$Q_{ij} = \begin{bmatrix} Q_{11} & Q_{12} & 0 \\ Q_{12} & Q_{22} & 0 \\ 0 & 0 & Q_{66} \end{bmatrix} \quad (7)$$

The stiffness coefficients of the above matrix can be calculated as

$$Q_{11} = \frac{E_L}{1 - \nu_{LT}\nu_{TL}}, Q_{12} = \frac{\nu_{TL}E_L}{1 - \nu_{LT}\nu_{TL}}, Q_{22} = \frac{E_T}{1 - \nu_{LT}\nu_{TL}}, Q_{66} = G_{LT} \quad (8)$$

As shown in Fig. 20c, the FDM printed overall part can be treated as a laminate composite with each printed layer equivalent to the individual lamina of the laminated plate. Therefore, the classical laminate theory (CLPT) can be applied to determine the mechanical behavior of printed parts. Combination of experimental and CLPT studies can be used to predict the properties of laminated parts [194]. Somireddy et al. investigated the mechanical behavior of the 3D printed short carbon fiber reinforced ABS composites using CLPT [195]. The modulus values E_L and E_T can be found experimentally by conducting tensile tests on a single layer FDM printed parts along 0° and 90° , respectively. The shear modulus G_{LT} is found from the laminate printed using symmetric laminate [+45/-45]s. The positions ratio is estimated by measuring the longitudinal and transverse strains using specimens printed at 0° raster orientation. Once the stiffness matrix in Eq. (7) is determined, the stiffness matrix of the certain layer of the laminate with arbitrary orientation θ can be found using

$$\overline{Q_{ij}} = [T]^{-1} [Q_{ij}] [T] \quad (9)$$

where T is the transformation matrix, which is given as,

$$T = \begin{bmatrix} \cos^2 \theta & \sin^2 \theta & \sin \theta \cos \theta \\ \sin^2 \theta & \cos^2 \theta & -\sin \theta \cos \theta \\ \sin \theta \cos \theta & -\sin \theta \cos \theta & \cos^2 \theta - \sin^2 \theta \end{bmatrix} \quad (10)$$

After finding the stiffness matrices of all layers of the laminate, the overall laminate behavior can be estimated using the constitutive equation,

$$\begin{Bmatrix} N \\ M \end{Bmatrix} = \begin{bmatrix} A & B \\ B & D \end{bmatrix} \begin{Bmatrix} \epsilon^0 \\ k \end{Bmatrix} \quad (11)$$

where N and M are the stress and moment resultants inside the laminate. The matrices A, B and D can be calculated as

$$A = \sum_{k=1}^n [\bar{Q}]_k (z_k - z_{k-1}), B = \frac{1}{2} \sum_{k=1}^n [\bar{Q}]_k (z_k^2 - z_{k-1}^2), D = \frac{1}{3} \sum_{k=1}^n [\bar{Q}]_k (z_k^3 - z_{k-1}^3) \quad (12)$$

where z is the distance of each layer from the laminate midplane. The elastic modulus along different directions of the overall laminate can be found from A, B, D matrices. The above discussed laminate plate theory reasonably estimates the mechanical behavior of the composite printed parts. Somireddy et al. used this theory to determine composite laminate

properties for two different layer thickness values [195]. The overall elastic modulus of the printed laminate predicted using CLPT is in close agreement with experimental for the parts printed using different layer thickness. The difference in the modulus is attributed to the presence of voids.

The CLPT approaches are limited to the ideal structures without voids. Hence, this analysis is restricted to the parts printed with zero airgaps and 100% infill ratio. However, as observed by many SEM images of the parts voids are inevitable during FDM printing. Further, the CLPT approaches can be applied for the layers along the thickness direction i.e. if the build orientation is flat. For edge and upright build orientations, the laminate theory cannot capture the mechanical behavior. Few works analyzed the elastic properties of the printed coupons using volume average stiffness (VAS) method [86,87]. In this method, the stiffness of the printed coupon is calculated by taking the volume average of stiffnesses of solid, infill and fiber regions. For example, the stiffness of a fiber reinforced composite printed part is calculated as

$$[Q_c] = V_m \bar{Q}_m + V_f \bar{Q}_f + V_{in} \bar{Q}_{in} \quad (13)$$

where V represents the volume fraction of each constituent. This approach can be used for calculating the elastic properties of continuous fiber reinforced composite printed parts. Further details of the application of this method can be found in Refs. [86,87].

In the micromechanics approach, the focus is on a repeating unit cell of the printed structure. In addition to the process modeling, FE based analysis can also be used to analyze the performance of the printed structures. These FE models can be categorized into models based on homogenized methods and models based on real microstructure. The homogenized models consider the effective properties of printed parts and the rasters are not explicitly molded [196,197]. In other models the real microstructure is considered in the analysis domain. Homogenization techniques are generally used to evaluate the constitutive behavior of composites from the properties and geometric features of its constituents. In these methods, a representative volume element (RVE) representing the periodic structure of the material is considered for the numerical analysis along with periodic boundary conditions. Somireddy et al. used these techniques to evaluate the constitutive behavior of the printed parts [198,199]. As shown in Fig. 29, two RVEs are considered from the L-shape printed part: one along the horizontal direction which represents the flat build orientation. The other one is taken along the vertical section which represents the upright built orientation. The FE analysis has been carried out on these two RVE by applying periodic boundary conditions. As an example, the response of two RVE domains under the axial strain is shown in Fig. 30. The calculated constitutive behavior is in good agreement with experimentally observed behavior.

4.3. Limitations of mathematical models

Even though existing models can reasonably capture the underlying physical phenomena, further work is required. In the process simulation, assumption of the melt as Newtonian fluid may not represent the anisotropic behavior of the melt flow caused by the presence of reinforcements. The size and shape of reinforcement affects the viscosity. The real composite material system may behave as non-Newtonian. Further work needs to be carried out to represent the flow behavior and fiber orientation accurately. Modeling reinforcements as discrete particles may accurately describe the flow induced fiber orientation, however, they are computationally expensive. The presence of fibers affects thermal properties and viscosities along printing and transverse directions. Previously presented viscous sintering models can be modified to incorporate the fiber effect on neck formation and growth. Modified models are also necessary to analyze the impregnation and bond strength of the continuous fiber reinforced composites printed using in-nozzle impregnation and/or separate print heads. The existing coupled thermal stress models have limitations to simulate the actual printing process of real life examples. The temperature dependence of the mechanical properties such as modulus and thermal expansion coefficients, and the polymer's viscoelastic nature must be considered. Also, during the printing of semi crystalline polymers, the properties are highly dependent on the degree of crystallinity. Considering all physical phenomena such as crystallization kinetics, solidification and viscoelastic material behavior in a single computational model is extremely difficult.

The analytical models for predicting properties of composites ignore voids in the composites. However, as discussed, composite printed parts contain considerable voids. Finite element computational models based on homogenization methods can be used. In these models, voids also can be considered in a RVE along with the real shape of the reinforcement. The analytical and homogenization methods discussed above can predict elastic properties of unreinforced printed parts to a great extent. Further work needs to be carried out in applying these models for analyzing the constitutive behavior of reinforced composite printed parts. Multiscale methods are generally used for analyzing the mechanical response of composites [200]. These models can accurately predict the mechanical behavior of printed composite parts. However, these methods are computationally intensive.

5. Summary, challenges and future scope

This paper presents an overview of the fused deposition modeling of thermoplastic composite materials. Various physical phenomena during printing that contribute to the strength of the printed parts have been explained clearly. The processing of composite filaments and the microstructural characteristics of the printed parts has been explained for a range of polymers; low strength amorphous polymers to high strength semi-crystalline polymers. Applications of the composite

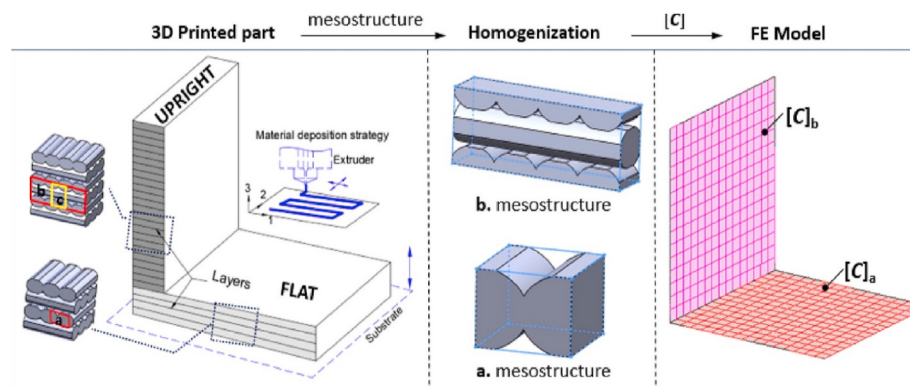


Fig. 29. 3D printed L-bracket structure with its mesostructure in a) horizontal plate b) vertical plate [198]. [Reprinted with permission].

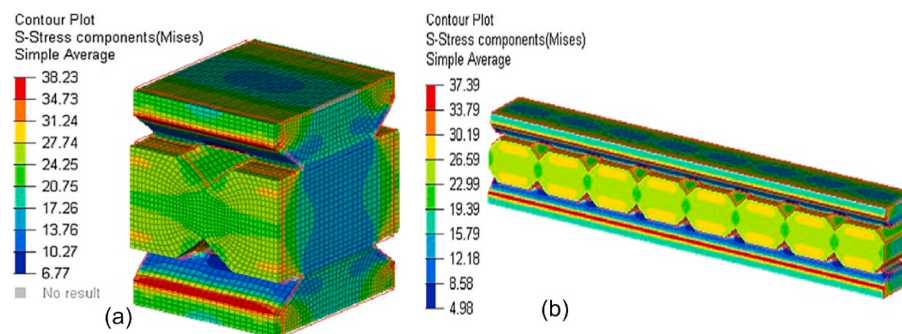


Fig. 30. Stress contours in (a) horizontal plate RVE (b) vertical plate RVE [198]. [Reprinted with permission].

printed parts in tooling, electronic, aerospace and biomedical fields are described. Mathematical models for simulating the printing process of composites and models for estimating the mechanical behavior of composites have been explained. Over the years, FDM has been portrayed as a promising technology, but many challenges still need to be overcome, especially for printing the polymer composites. The challenges and future directions are.

1. Materials: The potential of FDM for fabricating devices using composite materials opened up a lot of research activities in the area of applied materials science. Researchers are focusing on developing high performance composites by reinforcing different fillers into thermoplastic composites. Incorporation of fillers alters the viscosity and elastic modulus and makes the feedstock filament preparation challenging. Future studies on composite printing should focus on reducing the melt viscosity, incorporating plasticizers to enhance the flow, optimizing the nozzle system to achieve the required pressure drop. The other challenge is to minimize void formation during printing. The addition of reinforcements may increase the strength of the material system, but this increase is countered by the poor reinforcement/matrix interface, non uniform distribution of reinforcements, improper impregnation. These factors will contribute to additional void formation. Further research is necessary to identify suitable coupling agents to enhance the interface. Most of the research concentrated on improving the mechanical and electrical properties. Further work is required in the direction of biomedical applications. Few thermoplastics are not bio compatible and not environment friendly. Research has to be focused on printing with recyclable plastics. The addition of natural filler fillers may have processing difficulties, but the overall cost of the composite printing can be reduced. The addition of natural fillers such as TMP has a positive effect on the mechanical performance of PP and PE polymers. Further research is necessary to optimize the process for printing polymer composites with natural fillers. Most of the research work has been carried out on composites made of low strength amorphous polymers such as ABS and PLA. The printing process of high performance polymer composites such as PEI, PEEK needs to be optimized.

The FDM printing of continuous fiber reinforced composites is still at an early stage. The primary issue with the continuous fiber reinforced composite printing is the delamination. Improving the adhesion between the layers along the vertical direction still needs to be explored. To date, only a few thermoplastic materials with low processing temperatures (ABS, PLA, nylon) have been used. Further work needs to be carried out to overcome the challenges of impregnating high temperature polymers over reinforcements in the liquefier. Printing with two separate nozzles may provide the best solution for printing several polymers and reinforcements; however, the process needs to be optimized.

- 2 Material performance: The main research focus is to match the strength of printed parts to the conventional injection molded parts. The longitudinal strength of the short fiber reinforced composite printed materials has been increased several times, still not yet matched the strength of aerospace grade light metal alloys. This is due to the poor stress transfer at the discontinuous reinforcement-matrix interface and presence of voids in the printed material. If the strength matches with commercial light weight metals such as aluminum, polymer printed parts can be directly used in real time applications. The strength of the continuous fiber system is higher, but delamination problems have to be avoided in these composite printed parts. Another major issue is the limited strength in the transverse direction. If the length of the reinforced short fibers is more than the critical length, the overall performance of the composite can be increased. Printing of composites with optimum fiber lengths may yield easy processing with high mechanical properties opening the scope of FDM for a wide variety of applications. The unidirectional printed parts show high amount of anisotropy. Printing the continuous fibers at different angles in each layer to get the isotropic nature of the printed sample is difficult for high modulus fibers. Further work needs to be explored in printing isotropic components.

3. Modeling: The amount and distribution of short fiber reinforcements highly depend on the flow behavior in the nozzle. There is a further need to develop coupled fluid-thermal-mechanical computational models for understanding the flow and deformation behavior in the process. These models can help in understanding the process and suggest optimized methods to provide a way forward for improving the quality of the printed parts. Numerical models based on RVE can be further extended to include voids in the computational domain. The percentage of void content can be calculated from the SEM or μ -CT images. Incorporation of voids in the RVE model provides insight into the mechanical behavior of printed part under externally applied loads. Multiscale methods that link the atomic scale interactions (diffusion etc.) to meso/macroscale behavior should be developed for analyzing the behavior of printed parts.

Even though the FDM technology is growing at a rapid pace, this is yet to reach the industrial demand. With continuous successes in printing the parts with multi functionality and combining with digital manufacturing, FDM technique could outperform traditional manufacturing processes in terms of time and cost savings.

Declaration of competing interest

The authors declare that they have no known competing financial interests or personal relationships that could have appeared to influence the work reported in this paper.

Acknowledgements

The authors would like to acknowledge the funding received from Science and Engineering Research Board (SERB), Department of Science and Technology (DST), India through the project: ECR/2018/002281.

Appendix A. Supplementary data

Supplementary data to this article can be found online at <https://doi.org/10.1016/j.compositesb.2020.108336>.

References

- [1] Crump SS. United States patent (19) crump (54) apparatus and method for creating Three-Dimensional Objects 1992:5121329.
- [2] Turner BN, Strong R, Gold AS. A review of melt extrusion additive manufacturing processes: I. Process design and modeling. *Rapid Prototyp J* 2014;20:192–204. <https://doi.org/10.1108/RPJ-01-2013-0012>.
- [3] Turner BN, Strong R. A review of melt extrusion additive manufacturing processes: II. Materials, dimensional accuracy, and surface roughness. *Rapid Prototyp J* 2015;21:250–61. <https://doi.org/10.1108/RPJ-02-2013-0017>.
- [4] Kumar LJ, Krishnadas Nair CG. Current trends of additive manufacturing in the aerospace industry, in: *Advances in 3D printing & additive manufacturing Technologies*. Springer. 2017. p. 39–54.
- [5] Zadpoor AA, Malda J. Additive manufacturing of biomaterials, tissues, and organs. *Ann Biomed Eng* 2017;45:1–11. <https://doi.org/10.1007/s10439-016-1719-y>.
- [6] Masood SH, Song WQ. Development of new metal/polymer materials for rapid tooling using fused deposition modelling. *Mater Des* 2004;25:587–94. <https://doi.org/10.1016/j.matdes.2004.02.009>.
- [7] Lee J-Y, An J, Chua CK. Fundamentals and applications of 3D printing for novel materials. *Appl Mater Today* 2017;(7):120–33. <https://doi.org/10.1016/J.AMPT.2017.02.004>.
- [8] Sachs E, Cima M, Cornie J. Three-dimensional printing: rapid tooling and prototypes directly from a CAD model. *CIRP Ann* 1990;39:201–4. [https://doi.org/10.1016/S0007-8506\(07\)61035-X](https://doi.org/10.1016/S0007-8506(07)61035-X).
- [9] Brenken B, Barocio E, Favaloro A, Kunc V, Pipes RB. Fused filament fabrication of fiber-reinforced polymers: a review. *Add Manuf* 2018;21:1–16.
- [10] Cincinnati incorporated, big area additive manufacturing 3D printer.
- [11] Thermwood-CNC routers and large scale additive machines.
- [12] DeNardo NM. Additive manufacturing of carbon fiber reinforced thermoplastic composites. Master Thesis. Purde University; 2016.
- [13] Nieto DM, Lo'pez VC, Molina SI. Large-format polymeric pellet-based additive manufacturing for the naval industry. *Add Manuf* 2018;23:79–85.
- [14] Singh S, Ramakrishna S, Singh R. Material issues in additive manufacturing: a review. *J Manuf Process* 2017;25:185–200.
- [15] Bellehumeur C, Li L, Sun Q, Gu P. Modeling of bond formation between polymer filaments in the fused deposition modeling process. *J Manuf Process* 2004;6: 170–8.
- [16] Sun Q, Rizvi G, Bellehumeur C, Gu P. Effect of processing conditions on the bonding quality of FDM polymer filaments. *Rapid Prototyp J* 2008;14:72–80.
- [17] Gurrala PK, Regalla SP. Part strength evolution with bonding between filaments in fused deposition modelling. *Virtual Phys Prototyp* 2014;9:141–9.
- [18] Rahim T, Abdullah AM, Akil HM. Recent developments in fused deposition modelling based 3D printing of polymers and their composites. *Polym Rev* 2019; 59:589–624.
- [19] Kabir SMF, Mathur K, Seyam AFM. A critical review on 3D printed continuous fiber-reinforced composites: history, mechanism, materials and properties. *Compos Struct* 2020;232:111476.
- [20] Wang X, Jiang M, Zhou Z, Gou J, Hui D. 3D printing of polymer composites: a review and prospective. *Composites Part B* 2017;110:442–58.
- [21] Heller B, Smith DE, Jack DA. Effects of extrudate swell and nozzle geometry on fiber orientation in fused filament fabrication nozzle flow. *Add Manuf* 2016;12: 252–64.
- [22] Leigh SJ, Bradley RJ, Purcell C, Billson DR, Hutchins DA. A simple, low cost conductive composite material for 3D printing of electronic sensors. *PloS One* 2012;7:e49365..
- [23] Tekinalp HL, Kunc V, Velez-Garcia GM, Duty CE, Love LJ, Naskar AK, et al. Highly oriented carbon fiber-polymer composites via additive manufacturing. *Compos Sci Technol* 2014;(105):144–50. <https://doi.org/10.1016/J.COMPSITECH.2014.10.009>.
- [24] Matsuzaki R, Ueda M, Namiki M, Jeong T, Asahara H, Horiguchi K, et al. Three dimensional printing of continuous fiber composites by in-nozzle impregnation. *Sci Rep* 2016;6:23058y1.
- [25] Yang C, Tian X, Liu T, Cao Y, Li D. 3D printing for continuous fiber reinforced thermoplastic composites: mechanism and performance. *Rapid Prototyp J* 2017; 23:209–15.
- [26] Goh GD, Dikshit V, Nagalingam AP, Goh GL, Agarwala S, Sing SL, et al. Characterization of mechanical properties and fracture mode of additively manufactured carbon fiber and glass fiber reinforced thermoplastics. *Mater Des* 2018;137:79–89.
- [27] Markforged Inc., <https://3d.markforged.com/say-hello.html?mfa=ga-search>.
- [28] Venkataraman N, Rangarajan S, Matthewson MJ, Harper B, Safari A, Danforth SC, et al. Feedstock material property-process relationships in fused deposition of ceramics (FDC). *Rapid Prototyp J* 2000;6:244–53.
- [29] Rayegani F, Onwubolu GC. Fused deposition modelling (FDM) process parameter prediction and optimization using group method for data handling (GMDH) and differential evolution (DE). *Int J Adv Manuf Technol* 2014;73:509–19. <https://doi.org/10.1007/s00170-014-5835-2>.
- [30] Chacon JM, Caminero MA, Garcia-Plaza E, Nunez PJ. Additive manufacturing of PLA structures using fused deposition modelling: effect of process parameters on mechanical properties and their optimal selection. *Mater Des* 2017;124:143–57.
- [31] Parandoush P, Lin D. A review on additive manufacturing of polymer-fibercomposites. *Compos Struct* 2017;182:36–53.
- [32] Mohan N, Senthil P, Vinodh S, Jayanth N. A review on composite materials and process parameter optimisation for the fused deposition modelling process. *Virtual Phys Prototyp* 2017;12:47–59.
- [33] Ngo TD, Kashani A, Imbalzano G, Nguyen KTQ, Hui D. Additive manufacturing (3D printing): a review of materials, methods, applications and challenges. *Composites Part B* 2018;143:172–96.
- [34] Balla VK, Kate KH, Satyavolu J, Singh P, Tadimeti JGD. Additive manufacturing of natural fiber reinforced polymer composites: processing and prospects. *Composites Part B* 2019;174:106956.
- [35] El Moumen A, Tarafaoui M, Lafdi K. Additive manufacturing of polymer composites: processing and modeling approaches. *Composites Part B* 2019;171: 166–82.
- [36] Kalsoom U, Nesterenko PN, Paull B. Recent developments in 3D printable composite materials. *RSC Adv* 2016;6:60355.
- [37] van de Werken N, Tekinalp H, Khanbolouki P, Ozcan S, Williams A, Tehrani M. Additively manufactured carbon fiber reinforced composites: state of the art and perspective. *Add Manuf* 2020;31:100962.
- [38] Fallon JJ, McKnight SH, Bortner MJ. Highly loaded fiber filled polymers for material extrusion: a review of current understanding. *Add Manuf* 2019;30: 100810.
- [39] Blok LG, Logana ML, Yu H, Woods BKS. An investigation into 3D printing of fiber reinforced thermoplastic composites. *Add Manuf* 2018;22:176–83.
- [40] Mazzanti V, Malagutti L, Mollica FFDM. 3D printing of polymers containing natural fillers: a review of their mechanical properties. *Polymers* 2019;11:1094.
- [41] Liu Z, Wang Y, Wu B, Cui G, Guo Y, Yan C. A critical review of fused deposition modeling 3D printing technology in manufacturing polylactic acid parts. *Int J Adv Manuf Technol* 2019;102:2877–89.
- [42] Ahn S, Montero M, Odell D, Roundy S, Wright P. Anisotropic material properties of fused deposition modeling ABS. *Rapid Prototyp J* 2002;8:248–57. <https://doi.org/10.1108/13552540210441166>.
- [43] Dawoud M, Taha I, Ebied SJ. Mechanical behaviour of ABS: an experimental study using FDM and injection moulding techniques. *J Manuf Process* 2016;21: 39–45. <https://doi.org/10.1016/j.jmapro.2015.11.002>.
- [44] Zhong W, Li F, Zhang Z, Song L, Li Z. Short fiber reinforced composites for fused deposition modeling. *Mater Sci Eng, A* 2001;301:125–30. [https://doi.org/10.1016/S0921-5093\(00\)01810-4](https://doi.org/10.1016/S0921-5093(00)01810-4).
- [45] Shofner M, Rodriguez-Macias F, Vaidyanathan R, Barrera E. Single wall nanotube and vapour grown carbon fiber reinforced polymers processed by extrusion freeform fabrication. *Composites Part A Appl Sci Manuf* 2003;34:1207–17. <https://doi.org/10.1016/J.COMPOSITEA.2003.07.002>.
- [46] Shofner ML, Lozano K, Rodriguez-Macias FJ, Barrera EV. Nanofiber-reinforced polymers prepared by fused deposition modeling. *J Appl Polym Sci* 2003;89: 3081–90. <https://doi.org/10.1002/app.12496>.
- [47] Ning F, Cong W, Hu Y, Wang H. Additive manufacturing of carbon fiber-reinforced plastic composites using fused deposition modeling: effects of process parameters on tensile properties. *J Compos Mater* 2016;51:451–62. <https://doi.org/10.1177/0021998316646169>.
- [48] Zhang W, Cotton C, Sun J, Heider D, Gu B, Sun B, et al. Interfacial bonding strength of short carbon fiber/acrylonitrile-butadiene-styrene composites fabricated by fused deposition modeling. *Compos B Eng* 2017;2018(137):51–9. <https://doi.org/10.1016/J.COMPOSITEB.11.018>.
- [49] Love LJ, Kunc V, Rios O, Duty CE, Elliott AM, Post BK, Blue CA. The importance of carbon fiber to polymer additive manufacturing. *J Mater Res* 2017;29:1893–8.
- [50] Weng Z, Wang J, Senthil T, Wu L. Mechanical and thermal properties of ABS/montmorillonite nanocomposites for fused deposition modeling 3D printing. *Mater Des* 2016;102:276–83.
- [51] Young RJ, Kinloch IA, Gong L, Novoselov KS. The mechanics of graphene nanocomposites: a review. *Compos Sci Technol* 2012;72:1459–76.
- [52] Ojha K, Penumakala PK, Marrivada GV, Chaganti PK, Gupta AK. Processing of glass fiber pultruded composites using graphene nanoplatelets modified epoxy matrix. *Mater Today Proceed* 2019;18:3298–304.
- [53] Wei X, Li D, Jiang W, Gu Z, Wang X, Zhang Z, et al. 3D printable graphene composite. *Sci Rep* 2019;5:11181. <https://doi.org/10.1038/srep11181>.
- [54] Dul S, Fambri L, Pegoretti A. Fused deposition modelling with ABS-graphene nano composites. *Composites Part A* 2016;85:181–91.
- [55] Aumann C, Pongwisuthiruchte A, Pattanauwat P, Potiyaraj P. Fabrication of ABS/graphene oxide composite filament for fused filament fabrication 3D printing. *Adv. Mater. Sci. Engg* 2018;2830437.
- [56] Nikzad M, Masood SH, Sbarski I. Thermo-mechanical properties of a highly filled polymeric composites for Fused Deposition Modeling. *Mater Des* 2011;2011(32): 3448–56. <https://doi.org/10.1016/J.MATDES.01.056>.
- [57] Ryder MA, Lados DA, Iannacchione GS, Peterson AM. Fabrication and properties of novel polymer-metal composites using fused deposition modeling. *Compos Sci*

- Technol 2018;(158):43–50. <https://doi.org/10.1016/J.COMPSCTECH.2018.01.049>.
- [58] Torrado Perez AR, Roberson DA, Wicker RB. Fracture Surface Analysis of 3D-Printed tensile specimens of novel ABS-based materials. *J Fail Anal Prev* 2014;14: 343–53. <https://doi.org/10.1007/s11668-014-9803-9>.
- [59] Torrado AR, Shemelya CM, English JD, Lin Y, Wicker RB, Roberson DA. Characterizing the effect of additives to ABS on the mechanical property anisotropy of specimens fabricated by material extrusion 3D printing. *Addit Manuf* 2015;(6):16–29. <https://doi.org/10.1016/J.ADDMA.2015.02.001>.
- [60] Quill TJ, Smith MK, Zhou T, Baioumy MGS, Berenguer JP, Cola BA, et al. Thermal and mechanical properties of 3D printed boron nitride – ABS composites. *Appl Compos Mater* 2018;25:1205–17. <https://doi.org/10.1007/s10443-017-9661-1>.
- [61] Hwang S, Reyes El, Moon K sik, Rumpf RC, Kim NS. Thermo-mechanical characterization of metal/polymer composite filaments and printing parameter study for fused deposition modeling in the 3D printing process. *J Electron Mater* 2015;44:771–7. <https://doi.org/10.1007/s11664-014-3425-6>.
- [62] Khatri B, Lappi K, Habedank M, Mueller T, Megnini C, Hanemann T. Fused deposition modeling of ABS-barium titanate composites: a simple route towards tailored dielectric devices. *Polymers* 2018;10:666. <https://doi.org/10.3390/polym10060666>.
- [63] Osman M, Atia M. Investigation of ABS-rice straw composite feedstock filament for FDM. *Rapid Prototyp J* 2018;24:1067–75. <https://doi.org/10.1108/RPJ-11-2017-0242>.
- [64] Torres J, Cole M, Owji A, DeMastry Z, Gordon A. An approach for mechanical property optimization of fused deposition modeling with polylactic acid via design of experiments. *Rapid Prototyp J* 2016;22:387–404. <https://doi.org/10.1108/RPJ-07-2014-0083>.
- [65] Ferreira RTL, Amatice IC, Dutra TA, Bürger D. Experimental characterization and micrography of 3D printed PLA and PLA reinforced with short carbon fibers. *Compos B Eng* 2017;124:88–100. <https://doi.org/10.1016/j.compositesb.2017.05.013>.
- [66] Plymill A, Minneci R, Alexander Greeley D, Gritton J, Alexander D, Greeley D. Graphene PLA composite feedstock development for fused deposition Modeling. Thesis, univ. Tennessee. 2016.
- [67] Bustillos J, Montero D, Nautiyal P, Loganathan A, Boels B, Agarwal A. Integration of graphene in poly(lactic) acid by 3D printing to develop creep and wear-resistant hierarchical nanocomposites. *Polym Compos* 2018;39:3877–88. <https://doi.org/10.1002/pc.24422>.
- [68] MÁ Caminero, Chacón JM, García-Plaza E, Núñez PJ, Reverte JM, Becar JP. Additive manufacturing of PLA-based composites using fused filament fabrication: effect of graphene nanoplatelet reinforcement on mechanical properties, dimensional accuracy and texture. *Basel: Polymers*; 2019. p. 11. <https://doi.org/10.3390/polym11050799>.
- [69] Sweeney CB, Lackey BA, Teipel BR, Saeid MA, Moran AG, Achee TC, et al. Welding of 3D-printed carbon nanotube-polymer composites by locally induced microwave heating. *Sci Asia* 2017;3:e1700262. <https://doi.org/10.1126/sciadv.1700262>.
- [70] Ivanov E, Kotsilkova R, Xia H, Chen Y, Donato RK, Donato K, et al. PLA/Graphene/MWCNT composites with improved electrical and thermal properties suitable for FDM 3D printing applications. *Appl Sci* 2019;9:1209.
- [71] Dominguez-Robles J, Martin NK, Fong ML, Stewart SA, Irwin NJ, Rial-Hermida MI, et al. Antioxidant PLA composites containing Lignin for 3D printing applications: a potential material for healthcare applications. *Pharmaceutics* 2019;11:165.
- [72] Zhang H, Mao X, Du Z, Jiang W, Han X, Zhao D, et al. Three dimensional printed macroporous polylactic acid/hydroxyapatite composite scaffolds for promoting bone formation in a critical-size rat calvarial defect model. *Sci Technol Adv Mater* 2016;17:136–48.
- [73] Antoniac I, Popescu D, Zapciu A, Antoniac A, Miculescu F, Moldovan H. Magnesium filled polylactic acid (PLA) material for filament based 3D printing. *Materials* 2019;12:719.
- [74] Li N, Li Y, Liu S. Rapid prototyping of continuous carbon fiber reinforced polylactic acid composites by 3D printing. *J Mater Process Technol* 2016;238: 218–25. <https://doi.org/10.1016/j.jmatprotec.2016.07.025>.
- [75] Tian X, Liu T, Yang C, Wang Q, Li D. Interface and performance of 3D printed continuous carbon fiber reinforced PLA composites. *Composites Part A Appl Sci Manuf* 2016;(88):198–205. <https://doi.org/10.1016/J.COMPOSITESA.2016.05.032>.
- [76] Tian X, Liu T, Wang Q, Dilmurat A, Li D, Ziegmann G. Recycling and remanufacturing of 3D printed continuous carbon fiber reinforced PLA composites. *J Clean Prod* 2017;142:1609–18. <https://doi.org/10.1016/j.jclepro.2016.11.139>.
- [77] Masood S, Song W. Thermal characteristics of a new metal/polymer material for FDM rapid prototyping process. *Assemb Autom* 2005;25:309–15. <https://doi.org/10.1108/014451505105026451>.
- [78] Garg H, Singh R. Investigations for melt flow index of Nylon 6-Fe composite based hybrid FDM filament. *Rapid Prototyp J* 2016;22:338–43. <https://doi.org/10.1108/RPJ-04-2014-0056>.
- [79] Singh R, Singh S, Fraternali F. Development of in-house composite wire based feed stock filaments of fused deposition modelling for wear-resistant materials and structures. *Compos B Eng* 2016;(98):244–9. <https://doi.org/10.1016/J.COMPOSITESB.2016.05.038>.
- [80] Singh R, Singh N, Amendola A, Fraternali F. On the wear properties of Nylon 6-SiC-Al2O3 based fused deposition modelling feed stock filament. *Compos B Eng* 2017;(119):125–31. <https://doi.org/10.1016/J.COMPOSITESB.2017.03.042>.
- [81] Singh R, Bedi P, Fraternali F, Ahuja IPS. Effect of single particle size, double particle size and triple particle size Al2O3 in Nylon-6 matrix on mechanical properties of feed stock filament for FDM. *Compos B Eng* 2016;(106):20–7. <https://doi.org/10.1016/J.COMPOSITESB.2016.08.039>.
- [82] Abdullah AM, Tuan Rahim TNA, Mohamad D, Akil HM, Rajion ZA. Mechanical and physical properties of highly ZrO₂/β-TCP filled polyamide 12 prepared via fused deposition modelling (FDM) 3D printer for potential craniofacial reconstruction application. *Mater Lett* 2017;189:307–9. <https://doi.org/10.1016/j.matlet.2016.11.052>.
- [83] Zhu D, Ren Y, Liao G, Jiang S, Liu F, Guo J, et al. Thermal and mechanical properties of polyamide 12/graphene nanoplatelets nanocomposites and parts fabricated by fused deposition modeling. *J Appl Polym Sci* 2017;134:45332. <https://doi.org/10.1002/app.45332>.
- [84] Goh GD, Dikshit V, Nagalingam AP, Goh GL, Agarwala S, Sing SL, et al. Characterization of mechanical properties and fracture mode of additively manufactured carbon fiber and glass fiber reinforced thermoplastics. *Mater Des* 2018;(137):79–89. <https://doi.org/10.1016/J.MATDES.2017.10.021>.
- [85] Dickson AN, Barry JN, McDonnell KA, Dowling DP. Fabrication of continuous carbon, glass and Kevlar fibre reinforced polymer composites using additive manufacturing. *Addit Manuf* 2017;(16):146–52. <https://doi.org/10.1016/J.ADDMA.2017.06.004>.
- [86] Melenka GW, Cheung BKO, Schofield JS, Dawson MR, Carey JP. Evaluation and prediction of the tensile properties of continuous fiber-reinforced 3D printed structures. *Compos Struct* 2016;153:866–75. <https://doi.org/10.1016/j.compositstruct.2016.07.018>.
- [87] Al Abadi H, Thai HT, Paton-Cole V, Patel VI. Elastic properties of 3D printed fibre-reinforced structures. *Compos Struct* 2018;193:8–18.
- [88] Carneiro OS, Silva AF, Gomes R. Fused deposition modeling with polypropylene. *Mater Des* 2015;83:768–76.
- [89] Spoerl M, Sapkota J, Weingrill G, Fischinger T, Arbeiter F, Holzer C. Shrinkage and warpage optimization of expanded perlite filled polypropylene composites in extrusion based additive manufacturing. *Macromol Mater Eng* 2017;10:1700143.
- [90] Spoerl M, Savandaih C, Arbeiter F, Sapkota J, Holzer C. Optimization of mechanical properties of glass-spheres filled polypropylene composites for extrusion based additive manufacturing. *Polym Compos* 2019;40:638–51.
- [91] Spoerl M, Arbeiter F, Raguz I, Weingrill G, Fischinger T, Traxler G, et al. Polypropylene filled with glass spheres in extrusion based additive manufacturing: effect of filler size and printing chamber temperature. *Macromol Mater Eng* 2018;303:1800179.
- [92] Stoop D, Pickering K. Sustainable composite fused deposition modelling filament using recycled pre-consumer polypropylene. *Compos B Eng* 2018;135:110–8.
- [93] Tabone MD, Cregg JJ, Beckman EJ, Landis AE. Sustainability metrics: life cycle assessment and green design in polymers. *Environ Sci Technol* 2010;21:8264–9.
- [94] Schirmeister CG, Hees T, Licht EH, Mulhaupt R. 3D printing of high density polyethylene by filament fabrication. *Addit Manuf* 2019;28:152–9.
- [95] Bedi P, Singh R, Ahuja IPS. Investigations for tool life of 3D printed HDPE and LDPE composite based rapid tooling for thermoplastics machining applications. *Engg Res Express* 2019;1. 015003.
- [96] Olesik P, Godziersz M, Kozioł M. Preliminary characterization of novel LDPE based wear resistant composite suitable for FDM 3D printing. *Materials* 2019;12:2520.
- [97] Tarres Q, Melbo JK, Delgado-Aguilar M, Espinach FX, Mutje P, Chinga-Carrasco G. Bio-polyethylene reinforced with thermomechanical pulp fibers: Mechanical and micromechanical characterization and its application in 3D-printing by fused deposition modeling 2018;153:70–7.
- [98] Guessasma S, Belhabib S, Nouri H. Printability and tensile performance of 3D printed Polyethylene Terephthalate Glycol using fused deposition modeling. *Polymers* 2019;11:1220.
- [99] Szkydłanska K, Credo W, Osinski D. Selected mechanical properties of PETG 3D prints. *Procedia Eng* 2017;177:455–61.
- [100] Hamidi A, Tadesse Y. Single step 3D printing of bioinspired structures via metal reinforced thermoplastic and highly stretchable elastomer. *Compos Struct* 2019; 210:250–61.
- [101] Ferreira I, Vale D, Machado M, Lino J. Additive manufacturing of polyethylene terephthalate glycol/carbon fiber composites: an experimental study from filament to printed parts. *J Materials Design and Applications*. 2018.
- [102] Rinaldi M, Ghidini T, Cecchini F, Brandao A. Additive layer manufacturing of poly(ether ether ketone) via FDM. *Composites Part B* 2018;145:162–72.
- [103] Deng X, Zeng Z, Peng B, Yan S, Ke W. Mechanical properties optimization of PEEK via fused deposition modeling. *Materials* 2018;11:216–26.
- [104] Valerant B, Kadivnik Z, Brajlih T, Anderson A, Drstvensek I. Processing poly(ether ether ketone) on a 3D printer for thermoplastic modeling. *Mater Technol* 2013;47:715–21.
- [105] Wu W, Geng P, Li D, Zhao H, Zhang JZ. Influence of layer thickness and raster angle on the mechanical properties of 3D printed PEEK and a comparative mechanical study between PEEK and ABS. *Materials* 2015;8:5834–46.
- [106] Cicala G, Latteru A, Curto BD, Russo AL, Recca G, Fare S. Engineering thermoplastics for additive manufacturing: a critical perspective with experimental evidence to support functional applications. *J Appl Biomater Funct Mater* 2017;15:10–8.
- [107] Vaezi M, Shoufeng Y. Extrusion based additive manufacturing of PEEK for biomedical applications. *Virtual Phys Prototyp* 2015;10:123–35.
- [108] Yang C, Tian X, Li D, Cao Y, Zhao F, Shi C. Influence of thermal processing conditions in 3D printing on the crystallinity and mechanical properties of PEEK material. *J Mater Process Technol* 2017;248:1–7.
- [109] Kishore V, Chen X, Ajinjeru C, Hassen AA, Lindal J, Failla J, et al. Additive manufacturing of high performance semi crystalline thermoplastic and their

- composites, Proceedings of 27th annual international solid freeform fabrication symposium. 2017.
- [110] Beretta S, Davies R, Shyng YT, Wang Y, Ghita O. Fused deposition modelling of high temperature polymers: exploring CNT PEEK composites. *Polym Test* 2017; 63:251–62.
- [111] Gonçalves J, Lima P, Krause B, Pötschke P, Lafont U, Gomes JR, et al. Electrically conductive polyetheretherketone nanocomposite filaments: from production to fused deposition modeling. *Polymers* 2018;10:925. <https://doi.org/10.3390/polym10080925>.
- [112] Meng L, Xiaoyong T, Junfan S, Weijun Z, Dichen L, Yingjie Q. Impregnation and inter layer bonding behaviours of 3D printed continuous carbon fiber reinforced poly (ether ether ketone) composites. *Composites Part A* 2019;121:130–8.
- [113] Kim G, Barocio E, Pipes RB, Sterkenburg R. 3D printed thermoplastic polyurethane bladder for manufacturing of fiber reinforced composites. *Add Manuf* 2019;29:100809.
- [114] Lin X, Coates P, Hebda M, Wang R, Lu Y, Zhang L. Experimental analysis of the tensile property of FFF-printed elastomers. *Polym Test* 2020;90:106687.
- [115] Christ JF, Aliheidari N, Ameli A, Potschke P. 3D printed highly elastic strain sensors on multiwalled carbon nanotube/thermoplastic polyurethane nanocomposites. *Mater Des* 2017;131:394–401.
- [116] Jiang S, Liao G, Xu D, Liu F, Li W, Cheng Y, et al. Mechanical properties analysis of polyetherimide parts fabricated by fused deposition modeling. *High Perform Polym* 2019;31:97–106.
- [117] Smith WC, Dean RW. Structural characteristics of fused deposition modeling polycarbonate material. *Polym Test* 2013;32:1306–12.
- [118] Hill N, Haghi M. Deposition direction dependent failure criteria for fused deposition modeling polycarbonate. *Rapid Prototyp J* 2014;20:221–7.
- [119] Cantrell J, Rohde S, Damiani D, Gurnani R, DiSandro L, Anton J, et al. Experimental characterization of the mechanical properties of 3D printed ABS and polycarbonate parts. *Rapid Prototyp J* 2017;23:811–24.
- [120] Shemelya CM, Rivera A, Perez AT, Rocha C, Liang M, Yu X, et al. Characterization of a 3D printable tungsten–polycarbonate polymer matrix composite for space-based applications. *J Electron Mater* 2018;44:2598–607.
- [121] Haq RHA, Saidin W, Mat UW. Improvement of mechanical properties of polycaprolactone (PCL) by addition of nano-montmorillonite and hydroxyapatite. *Appl Mech Mater* 2013;315:815–9.
- [122] Davila J, Freitas M, Neto PI, Silveria Z, Silva J, dAvila M. Fabrication of PCL/β-TCP scaffolds by 3D mini extrusion printing. *J Appl Polym Sci* 2016;133.
- [123] Haleem A, Javaid M. Polyether ether ketone (PEEK) and its 3D printed implants applications in the medical field: an overview. *Clin Epidemiol Glob Heal* 2019;7: 571–7. <https://doi.org/10.1016/j.cegh.2019.01.003>.
- [124] Kumar YR. Bio-Modelling using rapid prototyping by fused deposition. *Adv Mater Res* 2012;488–489:1021–5. doi:10.4028/www.scientific.net/AMR.488-489.1021.
- [125] Kumar S, Kruth JP. Composites by rapid prototyping technology. *Mater Des* 2010; 31:850–6.
- [126] Zein I, Hutmacher DW, Tan KC, Teoh SG. Fused deposition modeling of novel scaffold architectures for tissue engineering applications. *Biomaterials* 2002;23: 1169–85.
- [127] Kalita SJ, Bose S, Hosick HL, Bandyopadhyay A. Development of controlled porosity polymer-ceramic composite scaffolds via fused deposition modelling. *Mater Sci Eng C* 2003;23:611–20. [https://doi.org/10.1016/S0928-4931\(03\)00052-3](https://doi.org/10.1016/S0928-4931(03)00052-3).
- [128] Kim J, McBride S, Tellis B, Alvarez-Urena P, Song YH, Dean DD, et al. Rapid-prototyped PLGA/β-TCP/hydroxyapatite nanocomposite scaffolds in a rabbit femoral defect model. *Biofabrication* 2012;4. <https://doi.org/10.1088/1758-5082/4/2/025003>.
- [129] Kabirian F, Ditzkowsky B, Zamanian A, Heying R, Mozafari M. An innovative approach towards 3D-printed scaffolds for the next generation of tissue-engineered vascular grafts. *Mater Today Proc* 2018;5:15586–94. <https://doi.org/10.1016/j.mtpr.2018.04.167>.
- [130] Woodfield TBF, Malda J, De Wijn J, Péters F, Riesle J, Van Blitterswijk CA. Design of porous scaffolds for cartilage tissue engineering using a three-dimensional fibre-deposition technique. *Biomaterials* 2004;25:4149–61. <https://doi.org/10.1016/j.biomaterials.2003.10.056>.
- [131] Zhang J, Zhao S, Zhu M, Zhu Y, Zhang Y, Liu Z, et al. 3D-printed magnetic Fe₃O₄/MBG/PCL composite scaffolds with multifunctionality of bone regeneration, local anticancer drug delivery and hyperthermia. *J Mater Chem B* 2014;2:7583–95.
- [132] Jakus AE, Secor EB, Rutz AL, Jordan SW, Hersam MC, Shah RN. Threedimensional printing of high-content graphene scaffolds for electronic and biomedical applications. *ACS Nano* 2015;9(4):4636e48.
- [133] Han X, Yang D, Yang C, Spintyzk S, Scheideler L, Li P, et al. Carbon fiber reinforced PEEK composites based on 3D-printing technology for orthopedic and dental applications. *J Clin Med* 2019;8:240.
- [134] Capel AJ, Rimington RP, Lewis MP, Christie SDR. 3D printing for chemical, pharmaceutical and biological applications. *Nat. Rev. Chem.* 2018;2:422–36.
- [135] Goyanes A, Chang H, Sedoughi D, Hatton GB, Wang J, Bunaz A, et al. Fabrication of controlled-release budesonide tablets via desktop (FDM) 3D printing. *Int J Pharm* 2015;496:414–20.
- [136] Castles F, Isakov D, Lui A, Lei Q, Dancer CEJ, Wang Y, et al. Microwave dielectric characterisation of 3D-printed BaTiO₃/ABS polymer composites. *Sci Rep* 2016;6: 1–8. <https://doi.org/10.1038/srep22714>.
- [137] Black Magic 3D. <https://graphene-supermarket.com/Conductive-Graphene-PLA-Filament.html>.
- [138] Proto-Pasta. <https://www.proto-pasta.com/pages/conductive-pla>.
- [139] Multi 3D. <https://www.multi3dlic.com/product/electrifi/>.
- [140] Flowers PF, Reyes C, Ye S, Kim MJ, Wiley BJ. 3D printing electronic components and circuits with conductive thermoplastic filament. *Addit Manuf* 2017;18: 156–63. <https://doi.org/10.1016/j.addma.2017.10.002>.
- [141] Kowk SW, Goh KHH, Tan ZD, Tan STM, Tjiu WW, Soh JY, et al. Electrically conductive filament for 3D-printed circuits and sensors. *Appl Mater Today* 2017; 9:167–75. <https://doi.org/10.1016/j.apmt.2017.07.001>.
- [142] Prashantha K, Roger F. Multifunctional properties of 3D printed poly(lactic acid)/graphene nanocomposites by fused deposition modeling. *J Macromol Sci Part A Pure Appl Chem* 2017;54:24–9. <https://doi.org/10.1080/10601325.2017.1250311>.
- [143] Zhang D, Chi B, Li B, Gao Z, Du Y, Guo J, et al. Fabrication of highly conductive graphene flexible circuits by 3D printing. *Synth. Mat* 2016;217:79–86.
- [144] Rymansaib Z, Iravani P, Emslie E, Martina M, Sak-Bosnar M, Verdejo R, et al. All polystyrene 3D-printed electrochemical device with embedded Carbon nanofiber-Graphite- Polystyrene composite conductor. *Elect. Anal.* 2016;28:1517–23.
- [145] Foster CW, Down MP, Zhang Y, Ji X, Rowley-Neale SJ, Smith GC, et al. 3D printed graphene based energy storage devices. *Sci Rep* 2017;7:42233. <https://doi.org/10.1038/srep42233>.
- [146] Foo CY, Lim HN, Mahdi MA, Wahid MH, Huang NM, Nay, et al. Three-dimensional printed electrode and its novel applications in electronic devices. *Sci Rep* 2018;8:1–11. <https://doi.org/10.1038/s41598-018-25861-3>.
- [147] Kim K, Park J, Suh J, Kim M, JeongY, Park I, 3D printing of multi axial force sensors using carbon nanotue (CNT)/thermoplastic polyurethane (TPU) filaments. *Sens. Actuators, A* 2017;263:493–500.
- [148] Hassen AA, Springfield R, Lindahl J, Post B, Love L, Duty C, et al. The durability of large-scale additive manufacturing composite molds. *CA: CAMX conf proc anaheim;* 2016.
- [149] Sudbury TZ, Springfield R, Kunc V, Duty C. An assessment of additive manufactured molds for hand-laid fiber reinforced composites. *Int J Adv Manuf Technol* 2017;90:1659–64.
- [150] Kunc V, Lindahl J, Dinwiddie R, Post B, Love L, Matlack M, et al. Investigation of in-autoclave additive manufacturing composite tooling. *CA: CAMX conf proc anaheim;* 2016.
- [151] Hassen AA, Lindahl J, Chen X, Post B, Love L, Kunc V. Additive manufacturing of composite tooling using high thermoplastic materials. *CA: SAMPE conf proc long beach;* 2016.
- [152] Duty CE, Kunc V, Compton B, Post B, Erdman D, Smith R, et al. Structure and mechanical behavior of big area additive manufacturing. *Rapid Prototyp J* 2017; 23:181–9.
- [153] Kunc V, Hassen AA, Lindahl J, Kim S, Post B, Love L. Large scale additively manufactured tooling for composites. *Sampe Conf Proc* 2017.
- [154] Klippstein H, Sanchez ADDD, Hassanin H, Zweiri Y, Seneviratne L. Fused deposition modeling for unmanned aerial vehicles (UAVs): a review. *Adv Eng Mater* 2017;1700552.
- [155] blog.stratasys.com/2015/11/09/aurora-uav-3d-printing/.
- [156] Gardner JM, Sauti G, Kim JW, Cano RJ, Wincheski RA, Stelter CJ, et al. 3D printing of multifunctional carbon nanotube yarn reinforced composites. *Add Manuf* 2016;12:38.
- [157] Goh GD, Agarwala S, Goh GL, Dikshit V, Sing SL, Yeong WY. Additive manufacturing in unmanned aerial vehicles (UAVs): challenges and potential. *Aero Sci Technol* 2017;63:140–51.
- [158] Azarov AV, Antonov FK, Golubev MV, Khaziev AR, Ushanov SA. Composite 3D printing for the small size unmanned aerial vehicle structure. *Composites Part B* 2019;169:157–63.
- [159] Duty CE, Ajinjeru C, Kishore V, Compton B, Hmeidat N, Chen X, et al. What makes a material printable? A viscoelastic model for extrusion based 3D printing of polymers. *J Manuf Process* 2018;35:526–37.
- [160] Mohamed OA, Masood SH, Bhowmik JL. Mathematical modeling and FDM process parameters optimization using response surface methodology based on Q-optimal design. *Appl Math Model* 2016;40:10052–73.
- [161] Compton BG, Post BK, Duty CE, Love L, Kunc V. Thermal analysis of additive manufacturing of large scale thermoplastic polymer composites. *Add Manuf* 2017;17:77–86.
- [162] Casavola C, Cazzato A, Moramarco V, Pappalettere C. Orthotropic mechanical properties of fused deposition modeling parts described by classical laminate theory. *Mater Des* 2016;90:453–8.
- [163] Nasirov A, Fidan I. Prediction of mechanical properties of fused filament fabricated structures via asymptotic homogenization. *Mech Mater* 2020;145: 103372.
- [164] Nixon J, Dryer B, Chiu D, Lempert I, Bigio DI, Three parameter analysis of fiber orientation in fused deposition modeling geometries.
- [165] Nikzad M, Masood SH, Sbarski I, Groth A. A study of melt flow analysis of an ABS-Iron composite in fused deposition modeling process,. *Tsinghua Sci Technol* 2009; 14:29–37.
- [166] Garcia A. Nozzle geometry effects on fiber orientation. *Sampe Conf Proc* 2017.
- [167] Heller B, Smith DE, Jack DA. Effects of extrudate swell and nozzle geometry on fiber orientation in fused filament fabrication nozzle flow. *Add Manuf* 2016;12: 252–64.
- [168] Lewicki JP, Rodriguez JN, Zhu C, Worsley MA, Wu A, Kanasra Y, et al. 3D-printing of meso-structurally ordered carbon fiber/polymer composites with unprecedented orthotropic physical properties. *Sci Rep* 2017;7:43401.
- [169] Aliheidari N, Triparaneni R, Ameli A, Nadimpalli S. Fracture resistance measurement of fused deposition modeling 3D printed polymers. *Polym Test* 2017;60:94–101.

- [170] Young D, Wetmore N, Czabaj M. Interlayer fracture toughness of additively manufactured unreinforced and carbon-fiber reinforced acrylonitrile butadiene styrene. *Addit Manuf* 2018;22:508–15.
- [171] Yıldırımcı M, Gucer S. Conceptual frame work for the thermal modeling of fused deposition. *Rapid Prototyp J* 1996;2:26–31.
- [172] Thomas JP, Rodriguez JF. Modeling the fracture strength between fused deposition extruded roads, Solid Free. *Fabr. SAVE Proc* 2000;17–23.
- [173] Penumakala PK, Nallathambi AK, Specht E, Bertram A. Mechanical behaviour of mushy zone in DC casting using a viscoplastic material model. *Techische Mech* 2012;32:342–57.
- [174] Divya PV, Penumakala PK, Nallathambi AK. Effect of wiper on thermal stress during the direct chill casting of magnesium alloys. *Mater Today Proceed* 2020.
- [175] Zhou Y, Nyberg T, Xiong G, Liu D. Temperature analysis in the fused deposition modeling process, *Int. Conf. Inf. Sci. Control Eng* 2016:678–82.
- [176] Costa SF, Duarte FM, Covas JA. Thermal conditions affecting heat transfer in FDM/FFF: a contribution towards the numerical modeling of the process. *Virtual Phys Prototyp* 2015;10:35–46.
- [177] Brenken B, Favaloro A, Barocio E, DeNardo NM, Pipes RB. Development of a model to predict temperature history and crystallization behaviour of 3D printed parts made from fiber reinforced thermos-plastics. *SAMPE Conf. Proc* 2016.
- [178] Velisaris C, Seferies J. Crystallization kinetics of polyetheretherketone (PEEK) matrices. *Polym.Engg. Sci.* 1986;26:1574–80.
- [179] Deiso G, Rebenfield L. Crystallization of fiber reinforced poly(phenylenesulfide) composites. II. Modeling the crystallization kinetics. *Appl. Polym. Sci.* 1992;45: 2005–20.
- [180] Brenken B, Barocio E, Favaloro A, Pipes RB. Simulation of semi crystalline composites in the extrusion deposition additive manufacturing processes. *Proc Sci Age Exp* 2017. Conf. by Dassault Syst.
- [181] Brenken B, Favaloro A, Barocio E, Pipes RB. Simulation of semi crystalline composite tooling made by extrusion deposition additive manufacturing processes. WA: SAMPE conf proc. Seattle; 2017.
- [182] Wang TM, Xi JT, Jin Y. A model research for prototype warp deformation in the FDM process, *Int. J Adv Manuf Technol* 2007;33:1087–96.
- [183] Xinhua L, Shengpeng L, Zhou L, Xianhua Z, Xiaohu C, Zhongbin W. An investigation on distortion of PLA thin-plate part in the FDM process. *Int J Adv Manuf Technol* 2015;79:1117–26.
- [184] Zhang Y, Chou K. A parametric study of part distortions in fused deposition modeling using three dimensional finite element analysis. *Proc Inst Mech Eng Part B J Eng Man* 2008;222:959–68.
- [185] Talagani MR, Dormohammadi S, Dutton R, Godines C, Baid H, Abdi F, et al. Numerical simulation of big area additive manufacturing (3D printing) of a full size car. *SAMPE J* 2015;51:27–36.
- [186] Li L, Sun Q, Bellehumeur C, Gu P. Composite modeling and analysis for fabrication of FDM prototypes. *J Manuf Process* 2002;4:129–41.
- [187] Croccolo D, De Agostinis M, Olmi G. Experimental characterization and analytical modeling of the mechanical behaviour of fused deposition modeling parts made of ABS-M30. *Comput Mater Sci* 2013;79:506–18.
- [188] Huang B, Singamneni S. Raster angle mechanics in fused deposition modeling. *J Compos Mater* 2014;49:363–83.
- [189] Reddy NS, Jinaga UK, Charukuri BR, Penumakala PK, Siva Prasad AVS. Failure analysis of AA8011-pultruded GFRP adhesively bonded similar and dissimilar joints 2019;90:97–105.
- [190] Agarwal BD, Broutman LJ, Chandrashekara K. Analysis and performance of fiber composites, 3rd edition. Wiley; 2006.
- [191] Mori T, Tanaka K. Average stress in matrix and average elastic energy of materials with misfitting inclusions. *Acta Metall* 1973;21:571–4.
- [192] Tandon GP, Weng GJ. The effect of aspect ratio of inclusions on the elastic properties of unidirectionally aligned composites. *Polym Compos* 1984;5:327–33.
- [193] Rodriguez JF, Thomas JP, Renaud JE. Characterization of the mesostructure of fused deposition acrylonitrile-butadiene-styrene materials. *Rapid Prototyp J* 2000;6:175–86.
- [194] Somireddy M, Czekanski A. Mechanical characterization of additively manufactured parts by FE modeling of mesostructure, *J. Manuf. Mater. Processes* 2017;1:18.
- [195] Somireddy M, Singh CV, Czekanski A. Mechanical behavior of 3D printed composite parts with short carbon fiber reinforcements. *Eng Fail Anal* 2020;107: 104232.
- [196] Domingo-Espin M, Puigoriol-Forcada JM, Garcia-Granada A-A Lluma J, Borros S, Reyes G, Mechanical property characterization and simulation of fused deposition modeling polycarbonate parts. *Mater Des* 2015;83:670–7.
- [197] Liu X, Shapiro V. Homogenization of material properties in additively manufactured structures. *CAD* 2016;78:71–82.
- [198] Somireddy M, Czekanski A, Singh CV. Development of constitutive material model of 3D printed structure via FDM. *Mater. Today Commun* 2018;15:143–52.
- [199] Somireddy M, Singh CV, Czekanski A. Analysis of material behavior of 3D printed laminates via FFF. *Exp Mech* 2019;59:871–81.
- [200] Kanoute P, Boso DP, Chaboche JL, Schrefler BA. Multiscale methods for composites: a review. *Arch Comput Methods Eng* 2009;16:31–75.